Statistical Theory and Related Fields

ISSN: 2475-4269 (Print) 2475-4277 (Online) Journal homepage: www.tandfonline.com/journals/tstf20

Uniform designs of experiments with mixtures under the mean L_1-distance criterion and a new approach to Scheffé-type designs

Yinan Li, Kai-Tai Fang & Yaping Wang

To cite this article: Yinan Li, Kai-Tai Fang & Yaping Wang (2026) Uniform designs of experiments with mixtures under the mean L_1-distance criterion and a new approach to Scheffé-type designs, Statistical Theory and Related Fields, 10:3, 383-412, DOI: 10.1080/24754269.2026.2689101

To link to this article: https://doi.org/10.1080/24754269.2026.2689101

Published online: 21 Jun 2026.

STATISTICAL THEORY AND RELATED FIELDS
2026, VOL. 10, NO. 3, 383–412
https://doi.org/10.1080/24754269.2026.2689101

Uniform designs of experiments with mixtures under the mean L_1-distance criterion and a new approach to Scheffé-type designs

Yinan Li[a,b], Kai-Tai Fang[a,c,d] and Yaping Wang [e]

[a]Department of Statistics and Data Science, Beijing Normal-Hong Kong Baptist University, Zhuhai, People's Republic of China; [b]Department of Mathematics, Hong Kong Baptist University, Hong Kong, People's Republic of China; [c]Guangdong Provincial Key Laboratory of Interdisciplinary Research and Application for Data Science, Zhuhai, People's Republic of China; [d]The Key Lab of Random Complex Structures and Data Analysis, The Chinese Academy of Sciences, Beijing, People's Republic of China; [e]KLATASDS-MOE, School of Statistics, East China Normal University, Shanghai, People's Republic of China

ABSTRACT

We introduce a criterion, named the mean L_1-distance (ML1D) criterion, to construct uniform designs in experiments with mixtures. This criterion allows for a flexible number of design points and produces a more uniform pattern within the experimental region, in terms of representative points of the uniform distribution across that region. We further explore the optimal Scheffé-type simplex-lattice designs under the ML1D criterion and show that a connection exists between uniform mixture designs and optimal Scheffé-type simplex-lattice designs. An efficient algorithm is proposed to generate uniform designs under the ML1D criterion. Simulations and applications highlight the advantages of the proposed designs, supporting their use for modelling and prediction in mixture experiments. Our method combines model-based and uniform design principles to enable flexible and efficient mixture experiments.

ARTICLE HISTORY
Received 30 June 2025
Accepted 10 June 2026

KEYWORDS
Experiments with mixtures; mean L_1-distance measure; Scheffé-type designs; representative points; uniform design with mixtures

1. Introduction

Experiments with mixtures are commonly employed in various fields, including chemistry, food science, pharmaceuticals, and materials science, where products are often composed of different components blended together. These experiments study how varying component proportions affect the response variable. Let x_i denote the proportion of the ith component, and then for a p-component system, a key feature of such experiments is that x_i must be non-negative and sum to one, restricting the design space to the p-dimensional simplex

$$T^p = \left\{ \left(x_1, \dots, x_p\right) : x_i \geqslant 0, 1 \leqslant i \leqslant p, \sum_{i=1}^{p} x_i = 1 \right\}. \tag{1}$$

The main objectives of conducting mixture experiments include (i) to identify optimal component combinations and proportions for achieving desired outcomes; (ii) to develop models

CONTACT Yaping Wang ypwang@fem.ecnu.edu.cn

This article was originally published with errors, which have now been corrected in the online version. Please see Correction (http://dx.doi.org/10.1080/24754269.2026.2721736)

describing the relationship between mixture components and response variables; and (iii) to use statistical methods for analysing experimental data and making predictions (Cornell, 2002).

Various designs for mixture experiments have been proposed, each originating from different considerations. Claringbold (1955) introduced a design based on the three-component simplex and provided the associated model fitting and data analysis. Scheffé (1958) proposed the widely-used simplex-lattice designs based on canonical polynomial regression models, laying the foundation for mixture designs. For a positive integer m, a $\{p, m\}$-simplex-lattice design consists of $\binom{p+m-1}{m}$ points in T^p, as illustrated in Figure 1(a). Notably, this number coincides with the number of coefficients in the associated canonical polynomial models, a fact that Scheffé (1958) highlighted to support the close alignment between polynomial regression methods and the simplex-lattice designs. Scheffé (1963) later introduced the simplex-centroid design, which consists of $2^p - 1$ points, including pure blends, binary, ternary mixtures, and the centroid point $(\frac{1}{p}, \dots, \frac{1}{p})$, shown in Figure 1(b). Cornell (1975) introduced the axial designs, where points are placed along the p axes of T^p, as shown in Figure 1(c). For comprehensive reviews of design and analysis of mixture experiments, see Cornell (1973, 2002, 2011).

Traditional mixture designs face two major limitations. First, most design points lie on the boundaries of the simplex (e.g., vertices, edges, or faces), making them unsuitable when strictly positive component levels are needed. Second, the number of design points is inflexible. For example, a three-component axial design has only 3 points, and simplex-lattice designs are constrained by the integer parameter m. To address the boundary-point issue, Wang and Fang (1990) and Fang and Wang (1994) suggested contracting the boundary points of simplex-lattice or simplex-centroid designs toward the centroid of T^p while maintaining the original design pattern. These contracted designs, referred to as Scheffé-type designs, aim to eliminate boundary points while distributing points more uniformly. Table 1 illustrates the $\{3, 3\}$-simplex-lattice design along with its Scheffé-type counterpart. The contraction parameter a is chosen to optimize uniformity. In the literature, some criteria under distance and uniformity are given. Fang and Wang (1994) considered using the mean squared error (MSE) to determine the optimal a. Prescott (2008) introduced designs under constrained ingredient bounds. Borkowski and Piepel (2009) used several distance-based metrics such as the root mean squared distance, the average distance, and the maximum distance. Ning et al. (2011) proposed optimizing a using the DM_2-discrepancy, a uniformity criterion defined directly on T^p.

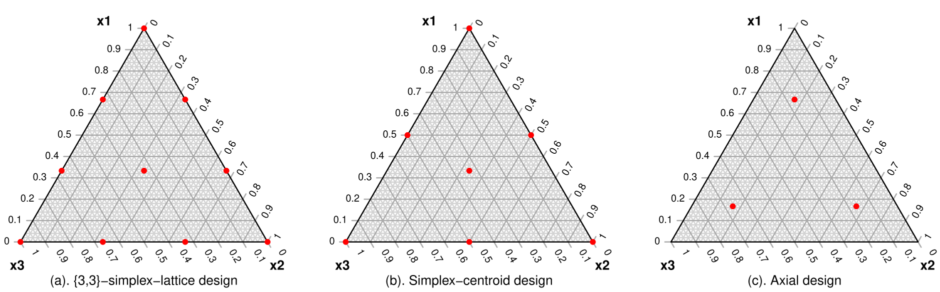

Figure 1. Examples of three traditional mixture designs with three components ($p = 3$).

Table 1. The $\{3,3\}$-simplex-lattice design and its contracted design.

No.	Simplex-lattice			Scheffé-type design ($a > 0$)		
	y_1	y_2	y_3	y'_1	y'_2	y'_3
1	1	0	0	$1-1/a$	$1/(2a)$	$1/(2a)$
2	0	1	0	$1/(2a)$	$1-1/a$	$1/(2a)$
3	0	0	1	$1/(2a)$	$1/(2a)$	$1-1/a$
4	2/3	1/3	0	$2/3-1/(2a)$	$1/3$	$1/(2a)$
5	1/3	2/3	0	$1/3$	$2/3-1/(2a)$	$1/(2a)$
6	2/3	0	1/3	$2/3-1/(2a)$	$1/(2a)$	$1/3$
7	1/3	0	2/3	$1/3$	$1/(2a)$	$2/3-1/(2a)$
8	0	2/3	1/3	$1/(2a)$	$2/3-1/(2a)$	$1/3$
9	0	1/3	2/3	$1/(2a)$	$1/3$	$2/3-1/(2a)$
10	1/3	1/3	1/3	$1/3$	$1/3$	$1/3$

However, Scheffé-type designs still suffer from a fixed number of design points. In practice, more flexible designs are often required. One solution introduced by Wang and Fang (1990) is to generate uniform designs on the unit cube $C^{p-1} = \{(x_1, \dots, x_{p-1}) : 0 \le x_i \le 1\}$ and map them to T^p, allowing any desired run size. But such transformations do not guarantee uniformity in T^p, although they ensures uniformity in C^{p-1}. An example is given in our simulation results (see Figure 4(a) in Section 5.1). To address this, Ning et al. (2011) proposed the DM_2-discrepancy, which generalizes the L_2-star discrepancy from the hypercube to the simplex. However, its computation is non-trivial, and the optimal design points obtained by this method may not exhibit a uniform pattern in T^p as anticipated.

An alternative perspective views the construction of mixture designs as selecting representative points (RPs) from the uniform distribution on the simplex T^p, denoted $U(T^p)$. Many criteria assess the closeness of these RPs to the target distribution (Fang & Pan, 2023). The two popular RPs are (i) Quasi-Monte Carlo RPs (QMC-RPs) generated using the F-discrepancy criterion, also known as the Kolmogorov–Smirnov distance, and (ii) minimum mean squared error RPs (MSE-RPs), which minimize the expected squared distance to the distribution. QMC-RPs have been shown to significantly improve the convergence of Monte Carlo estimates, with extensive applications in statistical inference, geometric probability, experimental design, and financial modelling (Fang & Wang, 1994; Fang et al., 1994; Pagès, 2018). When applied to experiments with mixtures, a set of uniform mixture designs can be regarded as a set of RPs under some criterion. Inspired by this perspective, we propose to use the *mean L_1-distance (ML1D) criterion* in this paper.

Many studies have examined the properties and generation of MSE-RPs for both univariate and multivariate distributions, including the normal (Fang & He, 1982), exponential (Xu et al., 2022), and two-component normal mixtures (Li et al., 2022), as well as elliptically contoured distributions (Yang et al., 2022). MSE-RPs have been applied to problems such as clothing standardization (Fang & He, 1982), mask design (Flury, 1990), signal transmission (Gray & Neuhoff, 1998), drug response classification (Tarpey & Petkova, 2010), and numerical integration (Pagès, 2018). The mean L_1-distance (ML1D), defined in Section 3, has been used in the construction of RPs (denoted by ML1D-RPs). Graf and Luschgy (2000) discussed the application of ML1D-RPs. Due to the nature of experiments with mixtures, we shall show that ML1D-RPs are more suitable. We propose an efficient algorithm for generating ML1D-RPs from $U(T^p)$ by utilizing its stochastic representation. The proposed mixture design offers three key advantages:

(1) Users can generate mixture design points of any size for a given number of components or ingredients using a straightforward algorithm.
(2) We explore the optimal Scheffé-type simplex-lattice designs under the ML1D criterion and identify connections with the ML1D-RPs derived from $U(T^p)$. When $p = 2$, we prove that the n ML1D-RPs are the optimal Scheffé-type $\{2, n-1\}$-simplex-lattice designs. For $p > 2$, we observe numerical equivalence between these two types of designs. This discovery shows that the new mixture uniform design keeps the optimality of the Scheffé simplex-lattice designs, thereby retaining their model-based advantages.
(3) Compared to the uniform mixture designs under other criteria, ML1D-RPs demonstrate improved representativeness of $U(T^p)$ when estimating the distribution mean vector and covariance matrix.

Mixture experiment design has primarily followed two main approaches: the model-driven simplex-lattice designs and the space-filling uniform designs. Simplex-lattice designs, as established by Scheffé (1958), are well-suited for precise model fitting but typically concentrate design points along the simplex boundaries, which can be problematic when strictly positive component levels are needed. On the other hand, uniform designs spread points more evenly throughout the entire experimental region, which improves coverage and increases robustness, yet these designs often lack the theoretical support of classical modelling approaches. The newly introduced ML1D criterion bridges these methods, integrating the structural and analytical benefits of simplex-lattice designs with the enhanced geometric uniformity of uniform designs. This unified approach delivers mixture experiment designs that are both flexible in structure and statistically robust.

The rest of the paper is organized as follows. Section 2 provides some preliminaries. Section 3 introduces uniform mixture designs under the ML1D criterion (ML1D-RPs from $U(T^p)$) and presents an efficient algorithm for generating ML1D-RPs. Theoretical results are developed in Section 4. Section 5 reports simulation studies, and Section 6 illustrates a modelling application. A discussion is given in Section 7. All proofs and additional tables and figures are provided in the Appendices.

2. Preliminaries

2.1. Stochastic representation of $U(T^p)$ and Monte Carlo RPs

Recall that the experimental factor domain of mixture designs is the simplex T^p, as defined in (1). To sample points within the target simplex, we need the Dirichlet distribution, which serves as a multivariate extension of the Beta distribution. This distribution is employed to characterize the probabilities associated with various outcomes.

Definition 2.1: Let $(Y_1, \ldots, Y_p)$ be a random vector. If it satisfies

(i) for any $1 \leqslant i \leqslant p$, $Y_i \geqslant 0$, and $\sum_{i=1}^{p} Y_i = 1$,

(ii) the probability density function of $(Y_1, \ldots, Y_{p-1})$ is

$$f\left(y_1, \ldots, y_{p-1}\right) = \begin{cases} \dfrac{\Gamma\left(\alpha_1 + \cdots + \alpha_p\right)}{\Gamma\left(\alpha_1\right) \cdots \Gamma\left(\alpha_p\right)} \prod_{i=1}^{p-1} y_i^{\alpha_i - 1} & \\ \times \left(1 - \sum_{i=1}^{p-1} y_i\right)^{\alpha_p - 1}, & \text{if } \left(y_1, \ldots, y_p\right) \in T_p, \\ 0, & \text{otherwise,} \end{cases}$$

then we say $(Y_1, \ldots, Y_p)$ follows a Dirichlet distribution, and denote it as $(Y_1, \ldots, Y_{p-1}) \sim \mathrm{Dir}_p(\alpha_1, \ldots, \alpha_{p-1}; \alpha_p)$ or $(Y_1, \ldots, Y_p) \sim \mathrm{Dir}_p(\alpha_1, \ldots, \alpha_p)$.

Notably, the uniform distribution $U(T^p)$ corresponds to a specific case of the Dirichlet distribution with $\alpha_i = 1, i = 1, \ldots, p$, and is widely recognized as a popular and important compositional distribution in T^p. When $p = 2$, the Dirichlet distribution $\mathrm{Dir}_2(\alpha_1, \alpha_2)$ is the Beta distribution, i.e., the Dirichlet distribution is an extension of the Beta distribution. Lemma 2.2 lists three useful properties of the Dirichlet distribution. Readers may refer to Johnson and Kotz (1972) and Fang et al. (1990) for further details.

Lemma 2.2: *Suppose* $(Y_1, \ldots, Y_p) \sim \mathrm{Dir}_p(\alpha_1, \ldots, \alpha_p)$, *where* $p \geq 2$. *Then* $(Y_1, \ldots, Y_p) \in T_p$, *and the following properties hold.*

(a) *There is a stochastic representation of Y_i's, that is,*

$$Y_i = \frac{X_i}{\sum_{j=1}^{p} X_j}, \quad i = 1, \ldots, p,$$

where $X_1, \ldots, X_p$ are independent random variables following Gamma distributions, $X_i \sim \mathrm{Ga}(\alpha_i, \lambda), \alpha_i > 0, \lambda > 0, i = 1, \ldots, p$, *with the probability density function*

$$\frac{\lambda_i^{\alpha}}{\Gamma(\alpha_i)} x^{\alpha_i - 1} \mathrm{e}^{-\lambda x} 1_{(0,\infty)}(x),$$

where $\Gamma(\cdot)$ is the gamma function and $1_A(\cdot)$ is the indicator function of A. When $\alpha_i = 1$, $\mathrm{Ga}(\alpha_i, \lambda)$ *reduces to the exponential distribution. The distribution of* $(Y_1, \ldots, Y_p)$ *is independent of λ.*

(b) *Denote* $\alpha = \sum_{i=1}^{p} \alpha_i$. *The lower marginal moments of* $(Y_1, \ldots, Y_p)$ *are*

$$E\left(Y_j\right) = \frac{\alpha_j}{\alpha}, \quad \mathrm{Var}\left(Y_j\right) = \frac{\alpha_j\left(\alpha - \alpha_j\right)}{\alpha^2(\alpha + 1)}, \quad \mathrm{Cov}\left(Y_i, Y_j\right) = \frac{-\alpha_i \alpha_j}{\alpha^2(\alpha + 1)}. \tag{2}$$

(c) $\mathrm{Dir}_p(1, \ldots, 1)$ *reduces to the uniform distribution* $U(T^p)$.

The following Lemma 2.3 from Fang and Fang (1988) is instrumental in our approach for generating mixture design points.

Lemma 2.3: *Suppose* $\boldsymbol{X} = (X_1, \ldots, X_p)$ *forms by p i.i.d. samples from the standard exponential distribution* $\mathrm{Exp}(1)$ *with probability density function* $f(x) = \mathrm{e}^{-x}$, *where* $x \geq 0$. *Let* $R = X_1 + \cdots + X_p$ *and* $\boldsymbol{U} = (U_1, \ldots, U_p) = \boldsymbol{X}/R$. *Then,*

(a) *$\boldsymbol{U} \sim U(T^p)$;*
(b) *R and $\boldsymbol{U}$ are independent;*
(c) *$\boldsymbol{X}$ has a stochastic representation: $\boldsymbol{X} \stackrel{d}{=} R\boldsymbol{U}$.*

Utilizing the stochastic representation of $U(T^p)$ given in Lemma 2.3, we recommend Algorithm 1 for generating random (Monte Carlo) samples from $U(T^p)$. These samples are hereafter referred to as MC-RPs.

Algorithm 1 Generate random samples (MC-RPs) from $U(T^p)$.

Step 1. Generate p random samples $e_1, \ldots, e_p$ from the standard exponential distribution Exp(1).
Step 2. Calculate $u = e_1 + \cdots + e_p$ and $u_i = e_i/u$ for $i = 1, \ldots, p$. Then, $\boldsymbol{u} = (u_1, \ldots, u_p)$ is a random sample from $U(T^p)$.
Step 3. Generate a set of n random samples from $U(T^p)$ by repeating Steps 1–2 n times.

2.2. QMC-RPs and MSE-RPs of $U(T^p)$

Two primary criteria, namely the F-discrepancy and the mean squared error (MSE), are employed to assess the representativeness of a set of points from the distribution $U(T^p)$ (Fang & Wang, 1994). The design points optimized under these criteria are referred to as QMC-RPs and MSE-RPs, respectively.

Fang and Wang (1994) suggested using number-theoretic methods (NTM) or called quasi-Monte Carlo (QMC) methods to generate uniform designs in T^p. These methods can significantly enhance the convergence rate of Monte Carlo estimates from $O(1/\sqrt{n})$ to $O(n^{-1}(\log n)^p)$ in statistical simulation and statistical inference, where n is the number of points in the simulation. The key technique of number-theoretic methods is to generate sets of points that are uniformly scattered on the unit cube C^p. For a comprehensive study and review, one can refer to Niederreiter (1992) and Fang and Wang (1994).

Let G be a finite region in $\mathbb{R}^p$. In the context of NTM, a set of points uniformly scattered in G is denoted as an NT-net in G. There are several methods for generating an NT-net. The good lattice point method, commonly used for generating NT-nets in C^p, has gained popularity. Fang and Wang (1994) presented detailed methods for generating NT-nets for various regions, including T^p. However, their methods involve more theoretical complexities and intricate algorithms. By leveraging the stochastic representation in Lemma 2.3 and the sampling efficiency of Algorithm 1, we suggest a more straightforward algorithm for generating QMC-RPs from the distribution $U(T^p)$, detailed in Algorithm 2.

In *Step 1* of Algorithm 2, we employ the good lattice point method to generate NT-nets in C^p. A comprehensive review of this method and its theoretical justification can be found in Fang and Wang (1994, subsection 1.3.1). *Step 2* employs the transformation from $\boldsymbol{C}$ to $\boldsymbol{Q}$ based on the correspondence between the uniform and exponential distributions: if $U \sim U(0, 1)$, then $-\log(U) \sim \text{Exp}(1)$. Using the stochastic representation in Lemma 2.3, this transformation yields a set of n QMC-RPs from $U(T^p)$.

Algorithm 2 Generate QMC-RPs from $U(T^p)$.

Step 1. Produce an NT-net on the unit cube C^p with n points. Denote the net as an $n \times p$ matrix $\mathbf{C} = (c_{ij})$, and then $c_{ij} \sim U(0,1)$.
Step 2. Calculate the matrix $\mathbf{Q} = (-\log(c_{ij})) \equiv (q_{ij})$ and produce the matrix $\boldsymbol{E} = (e_{ij} = \frac{q_{ij}}{q_i})$, where $q_i = q_{i1} + \cdots + q_{ip}$. Then, the n rows of $\boldsymbol{E}$ are a set of QMC-RPs from $U(T^p)$.

Since the exact value of the second criterion of uniformity measure (MSE) is challenging to compute directly, the Monte Carlo sampling method is commonly employed to obtain an approximate value. This method involves sampling a large number of points from the experimental region of interest. Fang and Wang (1994) introduced the NTLBG (Number-Theoretic Linde-Buzo-Gray) algorithm to find MSE-RPs from $U(T^p)$. This algorithm utilizes the number-theoretic method to generate a large set of points that are uniformly scattered (NT-net) in the region and can be used as a sampling set. Later, Ning et al. (2011) applied the NTLBG method to evaluate the uniform mixture designs under the MSE criterion. Based on their results from two real case examples, the NTLBG algorithm proves to be a good design construction approach for experiments with mixtures.

3. The mean L_1-distance (ML1D) criterion and an algorithm for generating ML1D-RPs

The mean L_1-distance (ML1D) is proposed to measure the representativeness of mixture design points from $U(T^p)$ in this paper.

Definition 3.1: For two points $\boldsymbol{x} = (x_1, \ldots, x_p)$ and $\boldsymbol{y} = (y_1, \ldots, y_p)$ in T^p, their L_1-distance is defined as

$$D_{l_1}(\boldsymbol{x}, \boldsymbol{y}) = \sum_{i=1}^{p} \left| x_i - y_i \right|.$$

Definition 3.2: Let $\mathcal{Y} = \{\boldsymbol{y}_1, \ldots, \boldsymbol{y}_n\} \subset T^p$ and $\boldsymbol{X} \sim U(T^p)$. Define a measure of uniformity of $\mathcal{Y}$ by

$$\mathrm{ML1D}(\mathcal{Y}) = E_{\boldsymbol{X}}\left[\min_{1\le j\le n} D_{l_1}\left(\boldsymbol{X}, \boldsymbol{y}_j\right)\right],$$

where the expectation is under the distribution of $\boldsymbol{X}$. A set with minimum value of ML1D is called ML1D-RPs in T^p with size n.

Similar to the computational complexity involved in MSE, direct computation of the exact ML1D value is analytically intractable. Motivated by the k-means algorithm and the NTLBG algorithm, we propose an efficient iterative procedure, Algorithm 3, to obtain design points with low ML1D values (ML1D-RPs) in T^p.

In Algorithm 3, Algorithms 1 and 2 play crucial roles. Algorithm 1 facilitates the generation of numerous Monte Carlo samples from $U(T^p)$, and Algorithms 1 and 2 contribute to setting up appropriate initial values for numerical search procedures.

Algorithm 3 Generate ML1D-RPs from $U(T^p)$.

Step 1. Prepare training samples:
Generate a set of N random samples $\mathcal{X} = \{\boldsymbol{x}_1, \ldots, \boldsymbol{x}_N\}$ *from* $U(T^p)$ *by Algorithm* 1, *where* N *is much larger than* n *and* p. *Let* $t = 0$.
Step 2. Set up initial ML1D-RPs (centroids), denoted by $\mathcal{Y}^{(t)} = \left\{\boldsymbol{y}_1^{(t)}, \ldots, \boldsymbol{y}_n^{(t)}\right\}$:
Method 1. Generate a set of n QMC-RPs from $U(T^p)$ *by Algorithm* 2 *as a set of initial seed points.*
Method 2. Generate a set of n QMC-RPs from $U(T^p)$ *by Fang and Wang's algorithm as a set of initial seed points.*
Method 3. Generate a set of n MC-RPs from $U(T^p)$ *by Algorithm* 1 *as a set of initial seed points.*
Step 3. Assign each training sample to the closest centroid:
Assign each point in $\mathcal{X}$ *into the nearest seed point by the* L_1*-distance to form sets of points* $G_j^{(t)}, j = 1, \ldots, n$, *i.e.,*

$$G_j^{(t)} = \left\{\boldsymbol{x} \in \mathcal{X} \mid D_{l_1}\left(\boldsymbol{x}, \boldsymbol{y}_j^{(t)}\right) < D_{l_1}\left(\boldsymbol{x}, \boldsymbol{y}_i^{(t)}\right), i \neq j\right\},$$

where each $\boldsymbol{x}$ *is assigned to exactly one* $G_j^{(t)}$. *Count the number of points in each* $G_j^{(t)}$ *and denote it as* $N_j^{(t)}$. *Calculate the corresponding ML1D by*

$$\mathrm{ML1D}^{(t)} = \frac{1}{N}\sum_{j=1}^{n}\sum_{\boldsymbol{x}_i \in G_j^{(t)}} \left|\boldsymbol{x}_i - \boldsymbol{y}_j^{(t)}\right|.$$

Step 4. Compute the new centroids:
Compute the mean of $G_j^{(t)}$, *for* $j = 1, \ldots, n$, *as the new seed points. Denote the new seed points as* $\boldsymbol{y}_1^{(t+1)}, \ldots, \boldsymbol{y}_n^{(t+1)}$.
Step 5. Stopping rule:
Repeat Steps 3–4 until

$$\frac{\mathrm{ML1D}^{(t)}}{N} - \frac{\mathrm{ML1D}^{(t+1)}}{N} < \epsilon,$$

where $\epsilon = 10^{-6}$ *is a tolerance value. Then, deliver* $\mathcal{Y}^{(t+1)} = \{\boldsymbol{y}_1^{(t+1)}, \ldots, \boldsymbol{y}_n^{(t+1)}\}$ *as ML1D-RPs. The corresponding probabilities of ML1D-RPs are* $\{p_j = N_j^{(t+1)}/N\}$.

In *Step 2* of Algorithm 3, three alternatives are provided for generating initial points for the iterative search. Methods 1 and 2 are recommended when the number of design points is available in NT-Net generation. Method 3 can be used to generate initial values for any specified number of points. It is important to note that the value of $\mathrm{ML1D}^{(t)}$ is non-increasing as t progresses from t to $t+1$ in Algorithm 3.

4. Theoretical results

In the previous section, we introduce uniform mixture designs under the ML1D criterion, referred to as ML1D-RPs from $U(T^p)$. Subsections 4.1–4.2 present theoretical results for ML1D-RPs within T^p. In Subsection 4.3, we investigate the optimal Scheffé-type simplex-lattice designs under the ML1D criterion and reveal their connection to ML1D-RPs.

4.1. Analytical solutions of one-point ML1D-RP within T^p

In this subsection, we investigate the ML1D-RP in the simplex T^p with size $n = 1$. Let $\boldsymbol{X} = (X_1, \ldots, X_p)$ represent a random vector in $\mathbb{R}^p$, and $\mathrm{Med}(X_i)$ denote the median of X_i. Under the L_1-norm, the spatial median $\mathbf{a} = (\mathrm{Med}(X_1), \ldots, \mathrm{Med}(X_p))$ (Graf & Luschgy, 2000, Sect. 2.2) satisfies

$$E|\boldsymbol{X} - \mathbf{a}| = \min_{\mathbf{b}\in\mathbb{R}^p} E|\boldsymbol{X} - \mathbf{b}|.$$

Hence, the spatial median $\mathbf{a}$ is equivalent to the ML1D-RP with a size of $n = 1$ for the random variable $\boldsymbol{X}$ in $\mathbb{R}^p$.

However, our interest lies in locating the ML1D-RP within the constrained domain T^p. Consider the random variable $\boldsymbol{Z} = (Z_1, \ldots, Z_p) \sim U(T^p)$ with $p \geq 2$. Each component Z_i follows a Beta distribution with the probability density function $f(z) = (p-1)(1-z)^{p-2}$ for $0 \leq z < 1$ and $1 \leq i \leq p$. The spatial median of $\boldsymbol{Z}$ is given by

$$\mathrm{Med}(Z_i) = 2^{-\frac{1}{p-1}}\left(2^{\frac{1}{p-1}} - 1\right), \quad \text{for } i = 1, \ldots, p.$$

When $p = 2$, this yields the point $(1/2, 1/2)$, which lies in T^2 and is the one-point ML1D-RP from $U(T^2)$. However, for $p > 2$, the spatial median of $\boldsymbol{Z} = (Z_1, \ldots, Z_p) \sim U(T^p)$ does not lie within T^p. For instance, we have $\mathrm{Med}(Z_i) = 1 - 1/\sqrt{2}$ when $p = 3$. While the point $(1 - 1/\sqrt{2}, 1 - 1/\sqrt{2}, 1 - 1/\sqrt{2})$ minimizes $E|\boldsymbol{z} - \mathbf{b}|$ for all $\mathbf{b} \in \mathbb{R}^3$, its components do not sum up to one, which is not desired for mixture experiments.

In Theorem 4.1, we establish that the centroid point $(1/p, \ldots, 1/p)$ serves as the one-point ML1D-RP within T^p and formulate the corresponding value of ML1D for any $p \geq 2$. The proof is given in Appendix 1, and Example 4.2 provides specific results for $p = 3$ and $p = 4$.

Theorem 4.1: *For any $p \geq 2$, the one-point ML1D-RP from $U(T^p)$ within T^p is*

$$\mathcal{Y}^* = \left\{\left(\frac{1}{p}, \ldots, \frac{1}{p}\right)\right\},$$

and the corresponding

$$\mathrm{ML1D}(\mathcal{Y}^*) = 2\left(1 - \frac{1}{p}\right)^p.$$

Example 4.2: When $p = 3$, we have $\mathcal{Y}^* = \{(1/3, 1/3, 1/3)\}$ and $\mathrm{ML1D}(\mathcal{Y}^*) = 16/27$. When $p = 4$, we have $\mathcal{Y}^* = \{(1/4, 1/4, 1/4, 1/4)\}$ and $\mathrm{ML1D}(\mathcal{Y}^*) = 81/128$.

4.2. Analytical solutions of ML1D-RPs on T^2

In this subsection, we explore the analytical solutions of ML1D-RPs for the case T^2. The simplex T^2 is essentially a line segment connecting the points $(0, 1)$ and $(1, 0)$. For uniform designs on the interval $[0, 1]$, Fang et al. (2002) demonstrated that under the centred L_2-discrepancy, the set

$$\left\{\frac{1}{2n}, \frac{3}{2n}, \ldots, \frac{2n-1}{2n}\right\}$$

is the uniquely optimal design of size n. Additionally, Fang and Wang (1994) highlighted that this design also stands as the unique uniform design when considering the L_2-star discrepancy.

Theorem 4.3: *For $p = 2$ and any $n \in \mathbb{N}^+$, the unique set of ML1D-RPs on T^2 of size n is*

$$\mathcal{Y}^* = \left\{\left(\frac{1}{2n}, \frac{2n-1}{2n}\right), \left(\frac{3}{2n}, \frac{2n-3}{2n}\right), \ldots, \left(\frac{2n-1}{2n}, \frac{1}{2n}\right)\right\},$$

with the corresponding $\mathrm{ML1D}(\mathcal{Y}^*) = 1/2n$.

Theorem 4.3 provides ML1D-RPs on T^2 of size n, which correspond to n equidistant points along this segment. The proof of Theorem 4.3 is available in Appendix 1. The subsequent discussion for the case of $p = 2$ and $n = 2$ provides some insight into the proof.

First, by Theorem 4.1 we know that, $\mathcal{Y}^* = \{(1/2, 1/2)\}$ is the ML1D-RP on T^2 of size $n = 1$. For the case with size $n = 2$, suppose $\boldsymbol{y}_1 = (x_1, 1 - x_1)$ and $\boldsymbol{y}_2 = (x_2, 1 - x_2)$ are two points on T^2, where $0 \le x_1 < x_2 \le 1$. Define $c = (x_1 + x_2)/2$ and $h = (x_2 - x_1)/2$, and then we can represent $\boldsymbol{y}_1$ and $\boldsymbol{y}_2$ as $\boldsymbol{y}_1 = (c - h, 1 - c + h)$ and $\boldsymbol{y}_2 = (c + h, 1 - c - h)$. The objective function to be minimized is

$$\begin{aligned}
\mathrm{ML1D}(\mathcal{Y}) &= E_{\boldsymbol{Z}}[\min_{1\le j\le 2} D_{l_1}(\boldsymbol{Z}, \boldsymbol{y}_j)] \\
&= \int_0^c (|z - (c - h)| + |1 - z - (1 - c + h)|)\, \mathrm{d}z \\
&\quad + \int_c^1 (|z - (c + h)| + |1 - z - (1 - c - h)|)\, \mathrm{d}z \\
&= 2\left(c^2 - c + 2h^2 - h + \frac{1}{2}\right),
\end{aligned}$$

where $\boldsymbol{Z} \sim U(T^2)$. By taking partial derivatives with respect to c and h, it is shown that the minimum value of $\mathrm{ML1D}(\mathcal{Y})$ is achieved precisely when $c = 1/2$ and $h = 1/4$. Therefore, the collection of ML1D-RPs for size $n = 2$ is given by $\mathcal{Y}^* = \{\boldsymbol{y}_1^* = (1/4, 3/4), \boldsymbol{y}_2^* = (3/4, 1/4)\}$ with $\mathrm{ML1D}(\mathcal{Y}^*) = 1/4$.

4.3. Optimal Scheffé-type simplex-lattice design under the ML1D criterion

The Scheffé-type simplex-lattice design was introduced in Section 1. Specifically, an illustrative example for the $\{3, 3\}$ case was provided in Table 1, where a is a contraction parameter that needs to be optimized. In fact, one can choose the ML1D criterion to optimize the parameter a for the Scheffé-type simplex-lattice design. Alternatively, we reformulate the contraction using a ratio parameter $\rho \in (0, 1]$, referred to as the *contraction ratio*, which offers a more interpretable geometric representation. Let $\mathcal{D} \subset T^p$ denote a simplex-lattice design in T^p and $\boldsymbol{y} = (y_1, \ldots, y_p)$ be a point of $\mathcal{D}$. Then a point $\boldsymbol{y}' = (y_1', \ldots, y_p')$ in the Scheffé-type simplex-lattice design corresponding to $\boldsymbol{y} \in \mathcal{D}$ can be determined by the following expression:

$$\boldsymbol{y}' - \frac{1}{p}\mathbf{1}_p = \rho\left(\boldsymbol{y} - \frac{1}{p}\mathbf{1}_p\right), \tag{3}$$

where $0 < \rho \leq 1$ is a parameter that we refer to as the contraction ratio. By (3), we have

$$y_i' = \rho y_i + \frac{1-\rho}{p}, \quad i = 1, \ldots, p.$$

We denote the contracted design of $\mathcal{D}$ as $\mathcal{D}_\rho$. Optimizing ρ is equivalent to optimizing a in a Scheffé-type simplex-lattice design. For instance, the relationship $\rho = 1 - 3/(2a)$ is valid for the Scheffé-type $\{3, 3\}$-simplex-lattice design in Table 1.

Unlike Scheffé-type simplex-lattice designs, which are constructed from geometric contractions, the uniform mixture designs under the ML1D criterion (called ML1D-RPs) are developed by directly minimizing a uniformity measure (the mean L_1-distance to the uniform distribution on T^p) for experimental points. Interestingly, we discover strong connections between ML1D-RPs and the Scheffé-type simplex-lattice designs even though these two types of designs are derived from different considerations.

ML1D-RPs on T^2 derived in Theorem 4.3 for the two-component mixture designs are considered as special cases of the Scheffé-type simplex-lattice designs. This is evident from the fact that a $\{2, m\}$-simplex-lattice design consists of $\binom{m+1}{m} = m + 1$ design points, which can be expressed as $\mathcal{D} = \{(0, 1), (1/m, 1 - 1/m), \ldots, (1, 0)\}$. Theorem 4.3 shows that the unique set of ML1D-RPs on T^2 is

$$\mathcal{Y}^* = \left\{\left(\frac{1}{2m+2}, \frac{2m+1}{2m+2}\right), \left(\frac{3}{2m+2}, \frac{2m-1}{2m+2}\right), \ldots, \left(\frac{2m+1}{2m+2}, \frac{1}{2m+2}\right)\right\}.$$

In this case, the set of ML1D-RPs $\mathcal{Y}^*$ is the contracted design $\mathcal{D}_\rho$ with the contraction ratio $\rho = m/(m + 1)$. We summarize this observation in the following corollary.

Corollary 4.4: *For $p = 2$ and any $n \geq 2$, the set of ML1D-RPs on T^2 of size n is a Scheffé-type $\{2, n - 1\}$-simplex-lattice design with the contraction ratio $\rho^* = (n - 1)/n$, where ρ^* is optimized under the ML1D criterion.*

Inspired by Corollary 4.4, we further observe that ML1D-RPs from $U(T^p)$ are numerically equivalent to the Scheffé-type simplex-lattice designs when $p > 2$ and the parameter a or ρ is optimized under the ML1D criterion. We call such designs optimal Scheffé-type simplex-lattice designs (OST-SLD) under the ML1D criterion. The following two-step procedure is used to generate such designs.

Step 1. Generate a $\{p, m\}$-simplex-lattice design $\mathcal{D}$ that has $n = \binom{p+m-1}{m}$ points.

Step 2. Identify the optimal contraction ratio ρ^* such that

$$\mathrm{ML1D}(\mathcal{D}_{\rho^*}) = \min_{0<\rho\leq 1} \mathrm{ML1D}(\mathcal{D}_\rho).$$

Output the optimal Scheffé-type simplex-lattice design (OST-SLD) $\mathcal{D}_{\rho^*}$.

In *Step 2*, it is essential to identify the optimal contraction ratio ρ^*. For $p = 3$, we derive the analytical solution for ρ^* and obtain a closed-form for $\mathrm{ML1D}(\mathcal{D}_{\rho^*})$, as given in the following Theorem.

Theorem 4.5: *Let $p = 3$ and $m \geq 1$. The optimal Scheffé-type $\{3, m\}$-simplex-lattice design under the ML1D criterion is $\mathcal{D}_{\rho^*}$ where*

$$\rho^* = \frac{m^2 - \sqrt{21m^2 + 102m + 81} + 10m + 9}{m^2 + 7m + 6}.$$

The corresponding ML1D is

$$\mathrm{ML1D}(\mathcal{D}_{\rho^*}) = \frac{7m^3 + 145m^2 - (14m + 54)\sqrt{21m^2 + 102m + 81} + 624m + 486}{9m(m+1)(m+6)^2}.$$

The proof of Theorem 4.5 can be found in Appendix 1. Example 4.6 lists the optimal 3-component Scheffé-type simplex-lattice designs for $n = 3, 6, 10$ and 15.

Example 4.6: Consider $p = 3$ and $m = 1, 2, 3, 4$. The following optimal Scheffé-type $\{3, m\}$-simplex-lattice designs are obtained by Theorem 4.5.

For $m = 1$, we have $\rho^* = (10 - \sqrt{51})/7$. The three design points are

$$\mathcal{D}_{\rho^*} = \left\{\left(\frac{27 - 2\sqrt{51}}{21}, \frac{\sqrt{51} - 3}{21}, \frac{\sqrt{51} - 3}{21}\right), \left(\frac{\sqrt{51} - 3}{21}, \frac{27 - 2\sqrt{51}}{21}, \frac{\sqrt{51} - 3}{21}\right),\right.$$
$$\left.\left(\frac{\sqrt{51} - 3}{21}, \frac{\sqrt{51} - 3}{21}, \frac{27 - 2\sqrt{51}}{21}\right)\right\}$$

with the corresponding $\mathrm{ML1D}(\mathcal{D}_{\rho^*}) = (631 - 68\sqrt{51})/441 \approx 0.3296664$. The numerical values of the design points can be found in Table A1 in Appendix 2.

For $m = 2$, we have $\rho^* = (11 - \sqrt{41})/8$. The six design points are

$$\mathcal{D}_{\rho^*} = \left\{\left(\frac{5}{4} - \frac{\sqrt{41}}{12}, \frac{\sqrt{41} - 3}{24}, \frac{\sqrt{41} - 3}{24}\right), \left(\frac{27 - \sqrt{41}}{48}, \frac{27 - \sqrt{41}}{48}, \frac{\sqrt{41} - 3}{24}\right),\right.$$
$$\left(\frac{\sqrt{41} - 3}{24}, \frac{5}{4} - \frac{\sqrt{41}}{12}, \frac{\sqrt{41} - 3}{24}\right), \left(\frac{\sqrt{41} - 3}{24}, \frac{27 - \sqrt{41}}{48}, \frac{27 - \sqrt{41}}{48}\right),$$
$$\left.\left(\frac{\sqrt{41} - 3}{24}, \frac{\sqrt{41} - 3}{24}, \frac{5}{4} - \frac{\sqrt{41}}{12}\right), \left(\frac{27 - \sqrt{41}}{48}, \frac{\sqrt{41} - 3}{24}, \frac{27 - \sqrt{41}}{48}\right)\right\}$$

with the corresponding $\mathrm{ML1D}(\mathcal{D}_{\rho^*}) = (395 - 41\sqrt{41})/576 \approx 0.2299859$. The numerical values of the design points can be found in Table A2 in Appendix 2.

Table 2. Comparisons of the optimal Scheffé-type $\{p, m\}$-simplex-lattice designs ($\mathcal{D}_{\rho^*}$) and ML1D-RPs ($\mathcal{Y}^*$) on the ML1D values, where $p = 3, n = \binom{p+m-1}{m}$, and ρ^* is the optimal contraction ratio under the ML1D criterion.

m	n	ρ^*	ML1D($\mathcal{D}_{\rho^*}$)	ML1D($\mathcal{Y}^*$)
1	3	0.4083674	0.3297	0.3295
2	6	0.5746095	0.2300	0.2300
3	10	0.6666667	0.1770	0.1769
4	15	0.7255437	0.1439	0.1438
5	21	0.7665669	0.1213	0.1222
6	28	0.7968365	0.1049	0.1049
7	36	0.8201124	0.0924	0.0929
8	45	0.8385778	0.0825	0.0829
9	55	0.8535898	0.0746	0.0750
10	66	0.8660376	0.0681	0.0681

For $m = 3$, we have $\rho^* = 2/3$. The ten design points of $\mathcal{D}_{\rho^*}$ are all possible combinations of the components under the constraint $x_1 + \cdots + x_p = 1$, and each component is an element from the set $\{1/9, 3/9, 5/9, 7/9\}$; see Table A3 in Appendix 2 for numerical values of the design points. The corresponding ML1D($\mathcal{D}_{\rho^*}$) $= 43/243 \approx 0.1769547$.

For $m = 4$, we have $\rho^* = (13 - \sqrt{33})/10$. The numerical values of the 15 points of $\mathcal{D}_{\rho^*}$ can be found in Table A4 in Appendix 2. The corresponding ML1D($\mathcal{D}_{\rho^*}$) $= (115 - 11\sqrt{33})/360 \approx 0.143916$.

It is noteworthy that all designs in Example 4.6 are numerically equivalent to ML1D-RPs on T^3 of the same point sizes obtained by Algorithm 3. Table 2 presents more comparison results between the two types of designs in the ML1D values. The optimal values of ρ^* for $m = 1, \ldots, 10$, along with the corresponding ML1D($\mathcal{D}_{\rho^*}$) values, are computed based on Theorem 4.5. For precise comparisons with the analytical solutions of the optimal Scheffé-type simplex-lattice designs, we generated ML1D-RPs using $N = 900{,}000$ Monte Carlo training samples from $U(T^3)$ by Algorithm 1.

Figure 2 compares simplex-lattice designs (SLD), Scheffé-type simplex-lattice designs (OST-SLD), and uniform mixture designs according to the ML1D criterion (ML1D-RPs) for $p = 3$ and $n = 6, 10, 15$ through a visual representation of the design points on T^3. The numerical values of ML1D-RPs can be found in Tables A1–A4 in Appendix 2. As observed in Figure 2, both OST-SLD and ML1D-RPs effectively contract the boundary points of the original simplex-lattice designs while maintaining the original SLD's structural patterns. The two designs follow the same contraction ratios, as is visually evident. In addition to visual comparison, we calculate the Frobenius norm, also known as the Hilbert-Schmidt norm, to quantitatively measure the distance between OST-SLD and ML1D-RPs given in Figure 2. For two $n \times p$ design matrices $\boldsymbol{X}$ and $\boldsymbol{Y}$, their Frobenius distance is defined as

$$||\boldsymbol{X} - \boldsymbol{Y}||_{\mathrm{F}} = \sqrt{\mathrm{tr}\left((\boldsymbol{X} - \boldsymbol{Y})^\top (\boldsymbol{X} - \boldsymbol{Y})\right)} = [\sum_{i=1}^{n} \sum_{j=1}^{p} (x_{ij} - y_{ij})^2]^{1/2}. \tag{4}$$

The computed Frobenius distances, presented in Table 3, reveal that the differences between these two design types are rather small. Both visual and numerical comparisons confirm that the design points of OST-SLD and ML1D-RPs are nearly identical.

Based on the analytical and numerical results in this subsection, we propose Conjecture 4.1.

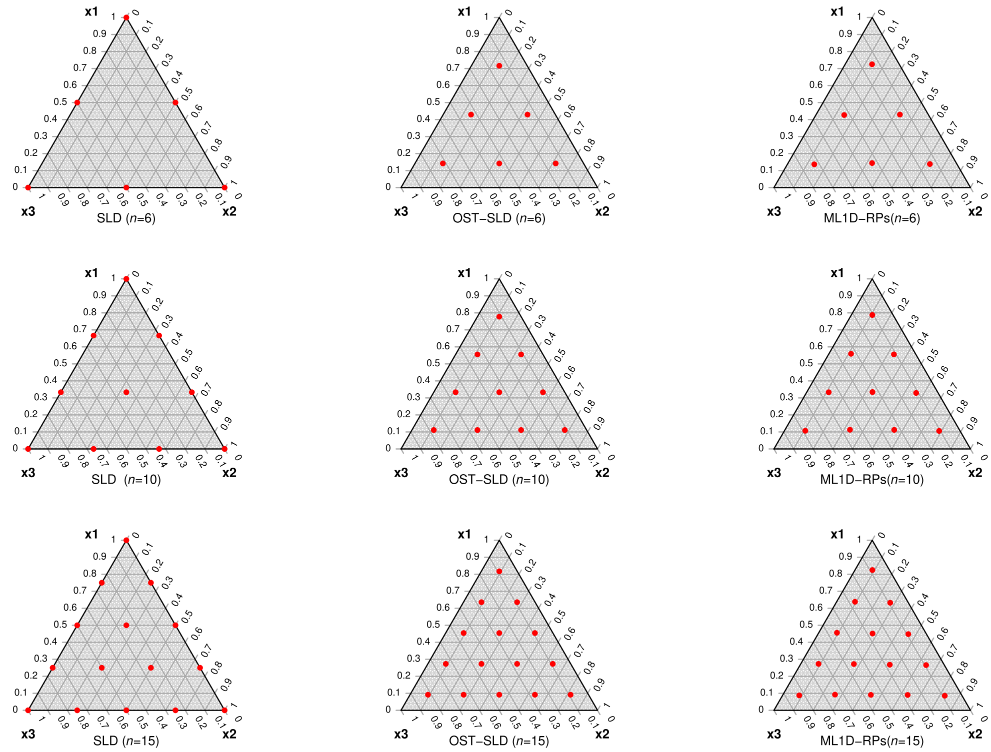

Figure 2. Comparisons of the simplex-lattice designs (SLD), the Scheffé-type simplex-lattice designs (OST-SLD) and the uniform mixture designs under the ML1D criterion (ML1D-RPs), where $p = 3$ and $n = 6, 10, 15$.

Table 3. Frobenius distance between the Scheffé-type simplex-lattice designs (OST-SLD) and the uniform mixture designs under the ML1D criterion (ML1D-RPs), where $p = 3$.

m	n	Frobenius distance
1	3	0.0119134
2	6	0.0196361
3	10	0.0228351
4	15	0.0299181

Conjecture 4.1: For $p \geq 2$, $m \geq 1$ and $n = \binom{p+m-1}{m}$, the optimal Scheffé-type $\{p, m\}$-simplex-lattice design generated by *Steps 1 and 2* is the set of ML1D-RPs from $U(T^p)$ of size n.

Remark 4.1: Corollary 4.4 confirms Conjecture 4.1 for $p = 2$. For $p = 3$, Theorem 4.5, together with the comparisons in Tables 2–3, Figure 2, and Tables A1–A4 in Appendix 2, strongly supports its validity. Further comparison results between the two types of designs when $p > 3$ are provided in Subsection 5.2.

Remark 4.2: Although we cannot prove Conjecture 4.1 for $p \geq 3$, one possible direction is to prove this conjecture in the asymptotic regime where n or $m \to \infty$. We conduct a numerical study by computing the mean L_1-distance (ML1D) criterion values for MC-RPs, ML1D-RPs, and optimal Scheffé-type $\{p, m\}$-simplex-lattice design (OST-SLD) for $n = \binom{p+m-1}{m}$, $m = 1, \ldots, 20$, $p = 3$. Figure A5 in Appendix 2 presents the ML1D value curves of these three types of RPs as a function of n. We observe that the curves for ML1D-RPs and OST-SLD are nearly identical and asymptotically coincident, while being distinctly separated from that of MC-RPs. This phenomenon can also be observed for $p = 4$ and 5.

The findings in this subsection show that ML1D-based uniform designs and Scheffé-type simplex-lattice designs complement each other well. While the former promotes geometric uniformity and flexibility, the latter preserves strong model-based interpretability (Scheffé, 1958). Their close agreement under the ML1D criterion provides both theoretical justification and practical value. These findings further support the unified framework proposed earlier, where ML1D-based designs combine the strengths of traditional model-based and space-filling methods, making them well suited for reliable modelling and prediction in mixture experiments.

5. Simulation

In this section, we evaluate five different types of representative points generated from $U(T^p)$:

(1) MC-RPs: the random samples generated from $U(T^p)$ using Algorithm 1.
(2) FW-QMC-RPs: the uniform mixture designs under F-discrepancy, generated based on the method of Fang and Wang (1994, Subsection 1.5.5).
(3) FF-QMC-RPs: the uniform mixture designs under F-discrepancy using Algorithm 2 (refer to Fang & Fang, 1988).
(4) MSE-RPs: the uniform mixture designs under the MSE criterion, generated based on the NTLBG algorithm.
(5) ML1D-RPs: the uniform mixture designs under the proposed ML1D criterion, generated by Algorithm 3.

Subsequently, we conduct a comparison between the uniform mixture designs under the ML1D criterion (ML1D-RPs from $U(T^p)$) and the optimal Scheffé-type designs when $p = 4, 5, 6$.

5.1. Comparisons among representative points from $U(T^p)$

To assess the performance of the five types of representative points from $U(T^p)$, we use the Euclidean distance to measure the difference between the sample mean vectors (SMV) and the theoretical mean vector (TMV), that is,

$$\|\text{SMV} - \text{TMV}\| = \left[\sum_{i=1}^{p} (\text{smv}_i - \text{tmv}_i)^2\right]^{1/2}. \tag{5}$$

Table 4. Comparison of the five types of representative points from $U(T^p)$, where $p = 3$, based on the estimation bias of the distribution mean vector and covariance matrix.

n	Measure	MC-RPs	FW-QMC-RPs	FF-QMC-RPs	MSE-RPs	ML1D-RPs
11	mean	0.1032	0.0057	0.0246	0.5624	0.0007
	covariance	0.0147	0.0277	0.0309	0.1153	0.0097
15	mean	0.0214	0.0025	0.0339	0.5624	0.0007
	covariance	0.0461	0.0188	0.0424	0.1153	0.0070
21	mean	0.0427	0.0072	0.0248	0.5624	0.0007
	covariance	0.0224	0.0173	0.0260	0.1152	0.0051
31	mean	0.0475	0.0271	0.0194	0.5624	0.0007
	covariance	0.0381	0.0341	0.0221	0.1152	0.0035

Table 5. Comparison of the five types of representative points from $U(T^p)$, where \$p= 4,5,10,15,20\$, based on the estimation bias of the distribution mean vector and covariance matrix.

p	n	Measure	MC-RPs	FW-QMC-RPs	FF-QMC-RPs	MSE-RPs	ML1D-RPs
4	22	mean	0.0299	0.0099	0.0072	0.0905	0.0044
		covariance	0.0301	0.0241	0.0136	0.0240	0.0095
4	50	mean	0.0334	0.0365	0.0097	0.0905	0.0044
		covariance	0.0285	0.0300	0.0222	0.0210	0.0056
5	50	mean	0.0271	0.0377	0.0118	0.4490	0.0035
		covariance	0.0227	0.0280	0.0186	0.4072	0.0084
5	97	mean	0.0370	0.0556	0.0114	0.4490	0.0035
		covariance	0.0242	0.0371	0.0132	0.4062	0.0061
10	101	mean	0.0437	0.0248	0.0156	0.0084	0.0076
		covariance	0.0122	0.0212	0.0122	0.0078	0.0038
15	113	mean	0.0264	0.0183	0.012	0.0056	0.0068
		covariance	0.0066	0.0157	0.0075	0.0061	0.0037
20	127	mean	0.0211	0.0133	0.0102	0.0035	0.0033
		covariance	0.0042	0.0118	0.0055	0.005	0.0031

We employ the Frobenius norm introduced in (4) to measure the distance between the sample covariance matrices (**SCM**) and the theoretical covariance matrix (**TCM**), i.e.,

$$||\mathbf{SCM} - \mathbf{TCM}||_{\mathrm{F}} = \sqrt{\mathrm{tr}\left((\mathbf{SCM} - \mathbf{TCM})^{\top}(\mathbf{SCM} - \mathbf{TCM})\right)}$$
$$= [\sum_{i=1}^{p}\sum_{j=1}^{p}(\mathrm{scm_{ij}} - \mathrm{tcm_{ij}})^2]^{1/2}. \tag{6}$$

The theoretical mean vector and covariance matrix of $U(T^p)$ are calculated using Lemma 2.2(b). It is important to note that the sample means, sample variances, and sample covariances of the two types of representative points, MSE-RPs and ML1D-RPs, rely on both the points and their corresponding probabilities. These probabilities are estimated by determining the occurrence of training samples within each cluster.

Table 4 presents the comparison results of the five types of representative points for the 3-component mixture design regarding the estimation bias of the mean vector and the covariance matrix of $U(T^p)$. The comparison results for the 4, 5, 10, 15 and 20-component mixture designs are presented in Table 5. The measure of 'mean' is calculated by (5) and the measure of 'covariance' is calculated using (6). Smaller values indicate more accurate estimation.

For 3-component mixture designs, FW-QMC-RPs outperform FF-QMC-RPs in moment estimations with point sizes of 11, 15, and 21 (see Table 4). Figure 3(a–b) illustrate that FW-QMC-RPs are more uniformly scattered than FF-QMC-RPs when $n = 11$ and $p = 3$. However, with $n = 31$, the performance in moment estimations of FF-QMC-RPs surpasses that of

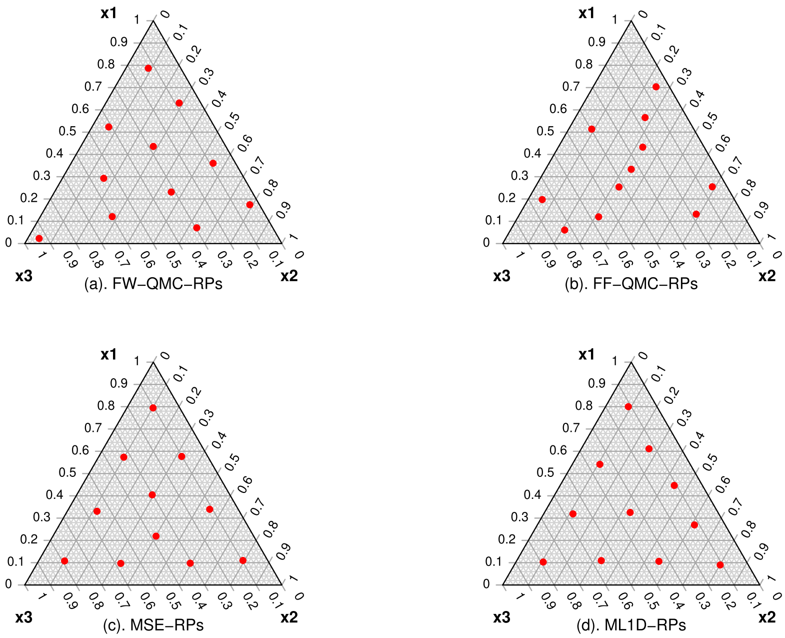

Figure 3. Four types of representative points ($n = 11, p = 3$).

FW-QMC-RPs. Visual comparisons are provided in Figure 4(a–b). When considering mixture designs with more than three components, FF-QMC-RPs outperform FW-QMC-RPs in moment estimations based on our simulation results (see Table 5). Therefore, Algorithm 2 is considered to be a good alternative to Fang and Wang's transformation algorithm for constructing uniform mixture designs under the F-discrepancy criterion.

For $p = 3, 4, 5, 10, 15, 20$, ML1D-RPs demonstrate superior estimation results for both mean vectors and covariance matrices across almost all examined point sizes compared to other types of points (see Tables 4 and 5). Note that the distances in mean vector estimation remain constant across different point sizes for MSE-RPs and ML1D-RPs. This consistency arises from the fact that these two types of points are derived from k-means clustering-based algorithms. Consequently, the sample mean vector of the design points matches the sample mean vector of the given training samples. For $p \geq 4$, we can give projection figures of different types of RPs. Figures A3 and A4 in Appendix 2 display the four types of representative points projected onto the first three and last three dimensions, respectively, for $n = 50$, $p = 4$. According to Figures 3, 4, A3 and A4, ML1D-RPs are distributed more uniformly and exhibit a more structured pattern. Based on the simulation results, we conclude that ML1D-RPs outperform the other RPs considered in this study. Therefore, we recommend using the uniform mixture design under the ML1D criterion, in conjunction with Algorithm 3.

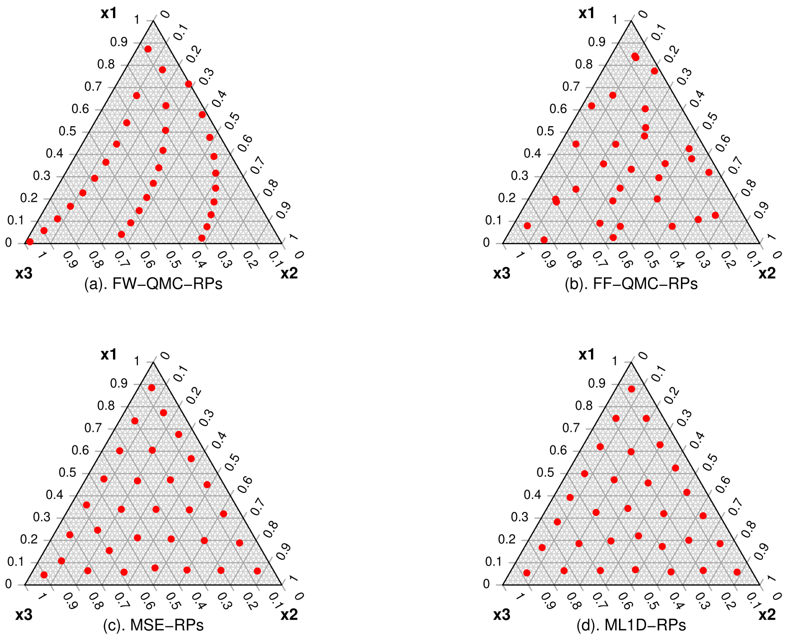

Figure 4. Four types of representative points ($n = 31, p = 3$).

5.2. More comparison results between the Scheffé-type simplex-lattice designs and ML1D-RPs from $U(T^p)$

In Subsection 4.3, we present a two-step approach for determining the optimal contraction ratio ρ^* of Scheffé-type simplex-lattice designs under the ML1D criterion. Closed-form solutions for ρ^* are derived for both $p = 2$ and $p = 3$. When $p \geq 4$, the optimal contraction ratio ρ^* can be obtained numerically by an algorithmic search in *Step 2*. To facilitate this process, we introduce Algorithm 4.

In *Step 3* of Algorithm 4, we employ the R function `optimize` for finding ρ^*. This function combines golden section search and successive parabolic interpolation for optimization (Brent, 1973). As a one-dimensional optimization problem, the speed of Algorithm 4 is fast.

We present comparisons between the Scheffé-type simplex-lattice designs and ML1D-RPs in ML1D values for $p = 4$, 5, 6. The results are shown in Table 6. The optimal values of ρ^* for Scheffé-type simplex-lattice designs are computed by Algorithm 4. Note that both types of designs use the same Monte Carlo training samples with a size of $N = 100{,}000$ for generating numerical design points, and thus share similar numerical approximation errors. According to Table 6, the ML1D values for both designs are nearly identical. For the small-sized case where $p = 4$, 5, 6 and $m = 1$ (i.e., $n = 4, 5, 6$, respectively), we also computed the Frobenius distances (see (4)) between the Scheffé-type simplex-lattice designs and ML1D-RPs in Table 7, which indicate that the points of the two types of designs are very close. These results support Conjecture 4.1.

Algorithm 4 Find the optimal contraction ratio ρ^* of the Scheffé-type simplex-lattice designs.

Step 1. Prepare training samples:
Generate a set of N random samples $\mathcal{X} = \{\boldsymbol{x}_1, \dots, \boldsymbol{x}_N\}$ from $U(T^p)$ by Algorithm 1, where N is much larger than n and p.
Step 2. Define the objective function:
Generate a $\{p, m\}$-simplex-lattice design $\mathcal{D}$, which has $n = \binom{p+m-1}{m}$ points. Generate the contracted design $\mathcal{D}_\rho = \{\boldsymbol{y}_{1,\rho}, \dots, \boldsymbol{y}_{n,\rho}\}$ where $\rho \in (0, 1)$. Assign each point in $\mathcal{X}$ into the nearest seed point by the L_1-distance to form sets of points $G_{j,\rho}, j = 1, \dots, n$, i.e.,

$$G_{j,\rho} = \left\{\boldsymbol{x} \in \mathcal{X} \mid D_{l_1}\left(\boldsymbol{x}, \boldsymbol{y}_{j,\rho}\right) < D_{l_1}\left(\boldsymbol{x}, \boldsymbol{y}_{i,\rho}\right), i \neq j\right\},$$

where each $\boldsymbol{x}$ is assigned to exactly one $G_{j,\rho}$. Define the objective function as

$$f(\rho) = \frac{1}{N}\sum_{j=1}^{n}\sum_{\boldsymbol{x}_i \in G_{j,\rho}} \left|\boldsymbol{x}_i - \boldsymbol{y}_{j,\rho}\right|.$$

Step 3. Search for the optimal contraction ratio ρ^*:
Use the R function `optimize` to search the interval $(0, 1)$ for a minimum of $f(\rho)$. Output the optimal ρ^*.

Table 6. Comparisons of the optimal Scheffé-type $\{p, m\}$-simplex-lattice designs ($\mathcal{D}_{\rho^*}$) and ML1D-RPs ($\mathcal{Y}^*$) on ML1D values, where $p = 4, 5, 6, n = \binom{p+m-1}{m}$, and ρ^* is the optimal contraction ratio searched by Algorithm 4 under the ML1D criterion.

p	m	n	ρ^*	ML1D($\mathcal{D}_{\rho^*}$)	ML1D($\mathcal{Y}^*$)
4	1	4	0.3550	0.3803	0.3803
	2	10	0.5157	0.2757	0.2824
	3	20	0.6103	0.2164	0.2162
	4	35	0.6740	0.1788	0.1798
5	1	5	0.3171	0.4166	0.4166
	2	15	0.4709	0.3105	0.3102
	3	35	0.5654	0.2489	0.2491
6	1	6	0.2879	0.4451	0.4450
	2	21	0.4347	0.3394	0.3437
	3	56	0.5286	0.2761	0.2754

6. Application

We illustrate the practical application of the proposed uniform mixture designs under the ML1D criterion by evaluating their performance in modelling and prediction tasks. Specifically, we consider three examples from the literature: a sweetness intensity model, a complex blending model and an eight-variable model modified from Example 1 of Loeppky et al. (2013). The sweetness intensity model, adapted from Cornell (2002) and Ruseckaite et al. (2017), involves blending glycine (x_1), saccharin (x_2), and an enhancer (x_3) to predict sweetness intensity. The true response surface is assumed to be

$$y = \beta_1 x_1 + \beta_2 x_2 + \beta_3 x_3 + \beta_{12} x_1 x_2 + \beta_{13} x_1 x_3 + \beta_{23} x_2 x_3 + \beta_{123} x_1 x_2 x_3, \tag{7}$$

Table 7. Frobenius distance between the Scheffé-type simplex-lattice designs (OST-SLD) and the uniform mixture designs under the ML1D criterion (ML1D-RPs), where $p = 4, 5, 6$ and $m = 1$.

p	m	n	Frobenius distance
4	1	4	0.0125817
5	1	5	0.0105115
6	1	6	0.0092259

where the coefficients $(\beta_1, \beta_2, \beta_3, \beta_{12}, \beta_{13}, \beta_{23}, \beta_{123})$ are drawn from a multivariate normal distribution with mean vector $(11.25, 5.54, 3.73, 26.93, 20.52, 28.44, -180.68)$ and covariance matrix $\sigma^2 I_7$, where $\sigma = 10$ and I_7 is the identity matrix.

The second model is a complex nonlinear blending model from Brown et al. (2015):

$$y = \beta_1 x_1 + \beta_2 x_2 + \beta_3 x_3 + \beta_{12} x_1 x_2^3 + \beta_{123} \frac{x_1^{2.5} x_2^{0.5} x_3^{0.5}}{x_1 + x_2 + x_3}. \tag{8}$$

This model, which also involves three mixture components x_1, x_2, x_3, features a highly asymmetric response surface with a strong joint effect of the components. The coefficients $(\beta_1, \beta_2, \beta_3, \beta_{12}, \beta_{123})$ are sampled from a multivariate normal distribution with mean vector $(3, 4, 5, 20, 80)$ and diagonal covariance matrix $\text{diag}\{1, 1, 1, 5, 20\}$.

The third model is modified from Example 1 of Loeppky et al. (2013), which involves eight variables $x_1, \ldots, x_8$. The true response function is assumed to be

$$y = \sum_{j=1}^{7} \beta_j x_j + \beta_{12} x_1 x_2 + \beta_{13} x_1 x_3 + \beta_{23} x_2 x_3 + \beta_{123} x_1 x_2 x_3, \tag{9}$$

where (x_1, x_2, x_3) would be highly sensitive, (x_4, x_5, x_6, x_7) would be moderately sensitive, and x_8 would be insensitive (note that it does not appear in (9)). The coefficients $(\beta_1, \ldots, \beta_7, \beta_{12}, \beta_{13}, \beta_{23}, \beta_{123})$ are drawn from a multivariate normal distribution with mean vector $(6, 4, 5.5, 2, 1, 0.4, 0.2, 3, 2.2, 1.4, 1)$ and covariance matrix $\sigma^2 I_{11}$, where $\sigma = 0.5$.

For all models, we assume the true response surfaces (7), (8) and (9) are unknown and generate data using various experimental designs. We fit the data using a widely used second-order Scheffé polynomial regression model $y = \sum_{i=1}^{p} \gamma_i x_i + \sum_{i=1}^{p-1} \sum_{j=i+1}^{p} \gamma_{ij} x_i x_j + \epsilon$, where γ_i and γ_{ij} represent the regression coefficients to be estimated, and ϵ denotes the error term, assumed to be normally distributed with mean zero and variance σ^2.

We compare seven types of designs: Scheffé-type simplex-lattice designs (OST-SLD), ML1D-RPs, MC-RPs, FW-QMC-RPs, FF-QMC-RPs, MSE-RPs, and Scheffé-type simplex-lattice designs (SLD) using the root mean squared error – RMSE $= [{n_t}^{-1} \sum_{i=1}^{n_t} (\hat{y}_i - y_i)^2]^{1/2}$ as the performance metric for prediction, where n_t is the number of data points in the test set, and $\hat{y}_i$ and y_i are the predicted and true responses, respectively, for the ith observation. We use a 100,000-run test set ($n_t = 100{,}000$) randomly drawn from $U(T^p)$, with $p = 3$ for Models (7)–(8) and $p = 8$ for Model (9).

In the simulation, we randomly generate the true parameters in Models (7), (8) and (9). We then generate the experimental designs and compute the true responses for each design. For the sweetness intensity model, designs are generated with run sizes $n = 10$ and $n = 15$. For the complex blending model, designs are generated with $n = 21$ and $n = 28$. For Model (9), designs are generated with $n = 36$ and $n = 120$. The second-order Scheffé regression model

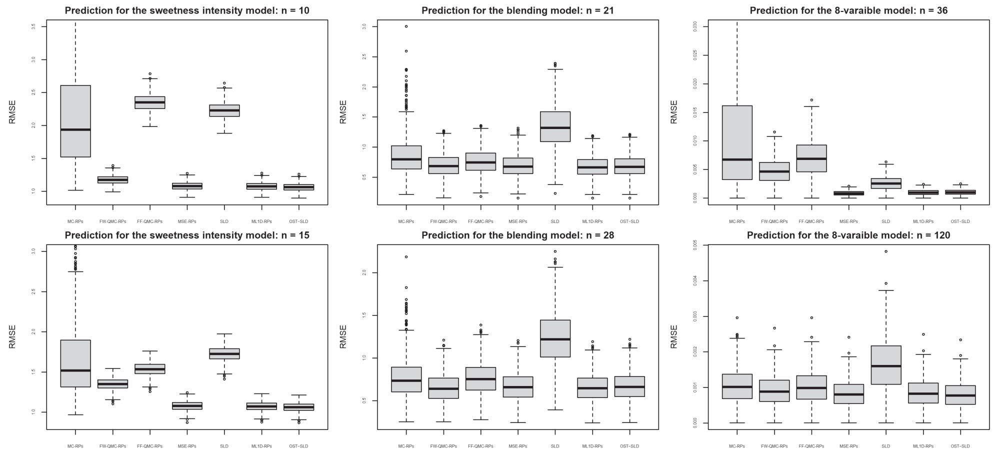

Figure 5. Comparison of RMSEs for the prediction of Models (7), (8) and (9) using different designs.

is fitted for each design, and the RMSE is computed by predicting the responses over the test set. This process is repeated 1000 times, and the resulting RMSE distributions are summarized with boxplots, as shown in Figure 5. The boxplots reveal that, across all cases, the OST-SLD, ML1D-RPs and MSE-RPs consistently yield smaller RMSEs than the other mixture designs. The performances of OST-SLD, ML1D-RPs and MSE-RPs are similar. Notably, OST-SLDs, constructed using an algebraic method, are computationally more efficient than MSE-RPs and ML1D-RPs, offering substantial savings in time while achieving comparable prediction performance. These results highlight the advantages of OST-SLDs in mixture experiments.

7. Discussion

In this paper, we introduce the mean L_1-distance (ML1D) criterion for constructing uniform designs (representative points) in mixture experiments. Efficient algorithms are proposed to generate uniform designs under the ML1D criterion. The resulting designs are flexible in point size and exhibit greater space-filling properties within the experimental region compared to existing designs. The obtained designs are actually representative points of the uniform distribution restricted within the domain T^p. Notably, the uniform distribution $U(T^p)$ belongs to the family of multivariate symmetric distributions related to the exponential distribution; see Fang and Fang (1988) for more details. For further study, it would be intriguing to obtain representative points of multivariate distributions related to the exponential distribution in $\mathbb{R}^p$.

We also investigate the optimal Scheffé-type simplex-lattice designs under the ML1D criterion. Interesting connections between the uniform mixture designs and the optimal Scheffé-type simplex-lattice designs are revealed (refer to Corollary 4.4, Theorem 4.5, Conjecture 4.1 and related simulations). The connections provide further rationale for using these designs in mixture experiments for modelling and prediction purposes. Our numerical findings lead us to believe that Conjecture 4.1 holds true for $p \geq 3$. However, it remains an open question to either provide a formal proof or discover a counterexample. For $p = 3$, Theorem 4.5 provides analytical solutions of the optimal Scheffé-type simplex-lattice designs under the ML1D criterion by using a Voronoi-cell method. It is possible to generalize this method to obtain similar analytical solutions for $p \geq 4$. Additionally, as one referee suggests, it may be possible to prove Conjecture 4.1 in the asymptotic regime where n or $m \to \infty$; see Remark 4.2.

It is worth noting that the Scheffé-type simplex-lattice designs are constrained to sizes $n = \binom{p+m-1}{m}$. In Figure A2 in Appendix 2, we offer the patterns of ML1D-RPs on T^3 for $p = 3$, $n = 4, \ldots, 15$. Some patterns similar to the Scheffé-type simplex-lattice designs are observed for $n \neq \binom{p+m-1}{m}$ (i.e., $n \neq 6, 10, 15$ in Figure A2). Understanding these patterns further may yield new design classes bridging structure and flexibility in mixture experiments.

Disclosure statement

No potential conflict of interest was reported by the author(s).

Funding

We are grateful to the editor, an associate editor and two reviewers for their insightful comments and constructive suggestions. This work was partially supported by the Guangdong Provincial Key Laboratory of Interdisciplinary Research and Application for Data Science, BNU-HKBU United International College (UIC) and UIC research grants [grant numbers 2022B1212010006 and R0400001-22], NSFC [grant numbers 12271166 and W2412023], National Key R&D Program of China [grant number 2024YFA1016200], and Young Elite Scientists Sponsorship Program by CAST [grant number 2022QNRC001].

ORCID

Yaping Wang http://orcid.org/0000-0002-2494-9072

References

Borkowski, J. J., & Piepel, G. F. (2009). Uniform designs for highly constrained mixture experiments. *Journal of Quality Technology*, *41*(1), 35–47. https://doi.org/10.1080/00224065.2009.11917758

Brent, R. (1973). *Algorithms for Minimization without Derivatives*. Prentice-Hall.

Brown, L., Donev, A. N., & Bissett, A. C. (2015). General blending models for data from mixture experiments. *Technometrics*, *57*(4), 449–456. https://doi.org/10.1080/00401706.2014.947003

Claringbold, P. J. (1955). Use of the simplex design in the study of joint action of related hormones. *Biometrics*, *11*(2), 174–185. https://doi.org/10.2307/3001794

Cornell, J. A. (1973). Experiments with mixtures: A review. *Technometrics*, *15*(3), 437–455. https://doi.org/10.1080/00401706.1973.10489071

Cornell, J. A. (1975). Some comments on designs for Cox's mixture polynomial. *Technometrics*, *17*(1), 25–35. https://doi.org/10.1080/00401706.1975.10489267

Cornell, J. A. (2002). *Experiments with Mixtures: Designs, Models, and the Analysis of Mixture Data*. Wiley.

Cornell, J. A. (2011). *A Primer on Experiments with Mixtures*. Wiley.

Fang, K. T., & Fang, B. Q. (1988). Some families of multivariate symmetric distributions related to exponential distribution. *Journal of Multivariate Analysis*, *24*(1), 109–122. https://doi.org/10.1016/0047-259X(88)90105-4

Fang, K. T., & He, S. (1982). The Problem of Selecting a Given Number of Representative Points in a Normal Population and a Generalized Mills' Ratio (Report No. SOLONR327). Stanford University CA Department of Statistics.

Fang, K. T., Kotz, S., & Ng, K (1990). *Symmetric multivariate and related distributions*. Chapman and Hall.

Fang, K. T., Ma, C. X., & Winker, P. (2002). Centered L_2-discrepancy of random sampling and Latin hypercube design, and construction of uniform designs. *Mathematics of Computation*, *71*(237), 275–296. https://doi.org/10.1090/S0025-5718-00-01281-3
Fang, K. T., & Pan, J. (2023). A review of representative points of statistical distributions and their applications. *Mathematics*, *11*(13), 2930. https://doi.org/10.3390/math11132930
Fang, K. T., & Wang, Y. (1994). *Number-Theoretic Methods in Statistics*. Chapman and Hall.
Fang, K. T., Wang, Y., & Bentler, P. M. (1994). Some applications of number-theoretic methods in statistics. *Statistical Science*, *9*(3), 416–428. https://doi.org/10.1214/ss/1177010392
Flury, B. D. (1990). Principal points. *Biometrika*, *77*(1), 33–41. https://doi.org/10.1093/biomet/77.1.33
Graf, S., & Luschgy, H. (2000). *Foundations of Quantization for Probability Distributions*. Springer-Verlag.
Gray, R., & Neuhoff, D. (1998). Quantization. *IEEE Transactions on Information Theory*, *44*(6), 2325–2383. https://doi.org/10.1109/18.720541
Johnson, N. L., & Kotz, S. (1972). *Distributions in Statistics: Continuous Multivariate Distributions*. Wiley.
Li, Y., Fang, K. T., He, P., & Peng, H. (2022). Representative points from a mixture of two normal distributions. *Mathematics*, *10*(21), 3952. https://doi.org/10.3390/math10213952
Loeppky, J. L., Williams, B. J., & Moore, L. M. (2013). Global sensitivity analysis for mixture experiments. *Technometrics*, *55*(1), 68–78. https://doi.org/10.1080/00401706.2012.727751
Niederreiter, H. (1992). *Random number generation and quasi-Monte Carlo methods*. Society for Industrial and Applied Mathematics. https://doi.org/10.1137/1.9781611970081.
Ning, J. H., Fang, K. T., & Zhou, Y. D. (2011). Uniform design for experiments with mixtures. *Communications in Statistics – Theory and Methods*, *40*(10), 1734–1742. https://doi.org/10.1080/03610921003637470
Ning, J. H., Zhou, Y. D., & Fang, K. T. (2011). Discrepancy for uniform design of experiments with mixtures. *Journal of Statistical Planning and Inference*, *141*(4), 1487–1496. https://doi.org/10.1016/j.jspi.2010.10.015
Pagès, G. (2018). *Numerical Probability: An Introduction with Applications to Finance*. Springer.
Prescott, P. (2008). Nearly uniform designs for mixture experiments. *Communications in Statistics – Theory and Methods*, *37*(13), 2095–2115. https://doi.org/10.1080/03610920701824257
Ruseckaite, A., Goos, P., & Fok, D. (2017). Bayesian D-optimal choice designs for mixtures. *Journal of the Royal Statistical Society: Series C (Applied Statistics)*, *66*(2), 363–386.
Scheffé, H. (1958). Experiments with mixtures. *Journal of the Royal Statistical Society. Series B (Methodological)*, *20*(2), 344–360. https://doi.org/10.1111/j.2517-6161.1958.tb00299.x
Scheffé, H. (1963). The simplex-centroid design for experiments with mixtures. *Journal of the Royal Statistical Society. Series B (Methodological)*, *25*(2), 235–263. https://doi.org/10.1111/j.2517-6161.1963.tb00506.x
Tarpey, T., & Petkova, E. (2010). Principal point classification: applications to differentiating drug and placebo responses in longitudinal studies. *Journal of Statistical Planning and Inference*, *140*(2), 539–550. https://doi.org/10.1016/j.jspi.2009.07.030
Wang, Y., & Fang, K. T. (1990). Number theoretic methods in applied statistics (II). *Chinese Annals of Mathematics, Series B*, *11*, 41–55.
Xu, L., Fang, K. T., & He, P. (2022). Properties and generation of representative points of the exponential distribution. *Statistical Papers*, *63*(1), 197–223. https://doi.org/10.1007/s00362-021-01236-1
Yang, J., He, P., & Fang, K. T. (2022). Three kinds of discrete approximations of statistical multivariate distributions and their applications. *Journal of Multivariate Analysis*, *188*, 104829. https://doi.org/10.1016/j.jmva.2021.104829

Appendix 1. Proofs

Proof of Theorem 4.1: Let $\boldsymbol{y} = (y_1, \ldots, y_p) \in T^p$, $\mathcal{Y} = \{\boldsymbol{y}\}$, $\boldsymbol{y}^* = (1/p, \ldots, 1/p)$ and $\mathcal{Y}^* = \{\boldsymbol{y}^*\}$. Let $\boldsymbol{Z} = (Z_1, \ldots, Z_p) \sim U(T^p)$ and μ denote the uniform distribution measure in T^p, and then

$$\mathrm{ML1D}(\mathcal{Y}) = E_{\boldsymbol{Z}}[D_{l_1}(\boldsymbol{Z}, \boldsymbol{y})] = \int_{(z_1,\ldots,z_p)\in T^p} \left(\sum_{i=1}^{p} |z_i - y_i| \right) \mathrm{d}\mu(\boldsymbol{z}).$$

Let τ denote a permutation of $(1, 2, \ldots, p)$, and then

$$\int_{(z_1,\ldots,z_p)\in T^p} \left(\sum_{i=1}^{p} |z_i - y_i|\right) \mathrm{d}\mu(\boldsymbol{z}) = \int_{(z_1,\ldots,z_p)\in T^p} \left(\sum_{i=1}^{p} |z_i - y_{\tau(i)}|\right) \mathrm{d}\mu(\boldsymbol{z})$$

because of the symmetry of T^p. Thus,

$$\begin{aligned}
p!\mathrm{ML1D}(\mathcal{Y}) &= \sum_{\tau} \int_{(z_1,\ldots,z_p)\in T^p} \left(\sum_{i=1}^{p} |z_i - y_{\tau(i)}|\right) \mathrm{d}\mu(\boldsymbol{z}) \\
&= \int_{(z_1,\ldots,z_p)\in T^p} \sum_{\tau} \left(\sum_{i=1}^{p} |z_i - y_{\tau(i)}|\right) \mathrm{d}\mu(\boldsymbol{z}) \\
&= \int_{(z_1,\ldots,z_p)\in T^p} \left(\sum_{i=1}^{p} \sum_{\tau} |z_i - y_{\tau(i)}|\right) \mathrm{d}\mu(\boldsymbol{z}) \\
&= \int_{(z_1,\ldots,z_p)\in T^p} \left(\sum_{i=1}^{p} (p-1)! \sum_{j=1}^{p} |z_i - y_j|\right) \mathrm{d}\mu(\boldsymbol{z}),
\end{aligned}$$

where $\sum_\tau$ means summing over by taking all possible $p!$ permutations of $(1, \ldots, p)$. Noting that $\sum_j y_j = 1$, we have

$$\sum_{j=1}^{p} |z_i - y_j| \geq |\sum_{j=1}^{p} z_i - \sum_{j=1}^{p} y_j| = p|z_i - 1/p|.$$

Therefore,

$$\mathrm{ML1D}(\mathcal{Y}) \geq \int_{(z_1,\ldots,z_p)\in T^p} \left(\sum_{i=1}^{p} |z_i - 1/p|\right) \mathrm{d}\mu(\boldsymbol{z}) = \mathrm{ML1D}(\mathcal{Y}^*).$$

As $Z_i \sim \mathrm{Beta}(1, p-1)$ for $i = 1, \ldots, p$ by Lemma 2.2, direct calculation gives

$$\mathrm{ML1D}(\mathcal{Y}^*) = p \int_0^1 |z - 1/p| \times (p-1)(1-z)^{p-2}\, \mathrm{d}z = 2(p-1)^p p^{-p},$$

which completes the proof. ■

Proof of Theorem 4.3: Suppose $\mathcal{Y} = \{\boldsymbol{y}_i = (y_i, 1 - y_i), i = 1, \ldots, n\}$ and $0 \leq y_1 < \cdots < y_n \leq 1$. Let $\boldsymbol{Z} \sim U(T^2)$. We prove the theorem by mathematical induction on n. We have shown the result for $n = 1, 2$ (see the last paragraph of Subsection 4.2). Suppose the conclusion holds for design size of $n - 1, n \geq 3$. For size n,

$$\begin{aligned}
\mathrm{ML1D}(\mathcal{Y}) &= E_{\boldsymbol{Z}}[\min_{1\leq j\leq n} D_{l_1}(\boldsymbol{Z}, \boldsymbol{y}_j)] \\
&= 2\Bigg(\int_0^{(y_1+y_2)/2} |z - y_1| \mathrm{d}z + \int_{(y_1+y_2)/2}^{(y_2+y_3)/2} |z - y_2|\, \mathrm{d}z \\
&\quad + \cdots + \int_{(y_{n-2}+y_{n-1})/2}^{(y_{n-1}+y_n)/2} |z - y_{n-1}| \mathrm{d}z + \int_{(y_{n-1}+y_n)/2}^{1} |z - y_n|\, \mathrm{d}z\Bigg).
\end{aligned}$$

Let us first suppose that $(y_{n-1} + y_n)/2 = c \in (0, 1)$ is fixed. Define

$$\begin{aligned}
g_c(y_1, \ldots, y_{n-1}) = 2\Bigg(&\int_0^{(y_1+y_2)/2} |z - y_1|\, \mathrm{d}z + \int_{(y_1+y_2)/2}^{(y_2+y_3)/2} |z - y_2|\, \mathrm{d}z \\
&+ \cdots + \int_{(y_{n-2}+y_{n-1})/2}^{c} |z - y_{n-1}|\, \mathrm{d}z\Bigg).
\end{aligned}$$

We have

$$g_c(y_1,\dots,y_{n-1})/c = 2\left(\int_0^{(y_1+y_2)/2} |z/c-y_1/c|\,\mathrm{d}z + \int_{(y_1+y_2)/2}^{(y_2+y_3)/2} |z/c-y_2/c|\,\mathrm{d}z + \cdots + \int_{(y_{n-2}+y_{n-1})/2}^{c} |z/c-y_{n-1}/c|\mathrm{d}z\right)$$
$$= 2c\left(\int_0^{(y_1/c+y_2/c)/2} |z'-y_1/c|\,\mathrm{d}z' + \int_{(y_1/c+y_2/c)/(2)}^{(y_2/c+y_3/c)/2} |z'-y_2/c|\,\mathrm{d}z' + \cdots + \int_{(y_{n-2}/c+y_{n-1}/c)/2}^{1} |z'-y_{n-1}/c|\mathrm{d}z'\right),$$

where in the last equality we let $z'=z/c$. Obviously, $g_c(y_1,\dots,y_{n-1})/c^2$ can be viewed as the ML1D of the set of points $\{(y_i/c, 1-y_i/c), i=1,\dots,n-1\}$ on T^2 for the distribution $U(T^2)$. By the assumption, $g_c(y_1,\dots,y_{n-1})/c^2$ is minimized if and only if $y_1/c=1/[2(n-1)]$, $y_2/c=3/[2(n-1)],\dots$, $y_{n-1}/c=(2n-3)/[2(n-1)]$, and the corresponding minimum value of $g_c(y_1,\dots,y_{n-1})$ is $\frac{c^2}{2(n-1)}$.

Now we optimize ML1D($\mathcal{Y}$) with respect to c and y_n. We have $0<c<y_n<1$ and

$$\mathrm{ML1D}(\mathcal{Y}) = \frac{c^2}{2(n-1)} + 2\int_c^1 |z-y_n|\,\mathrm{d}z = \frac{c^2}{2(n-1)} + c^2 - 2cy_n + 2y_n^2 - 2y_n + 1.$$

Taking partial derivative of y_n and c, we obtain that the minimum of ML1D($\mathcal{Y}$) is attained at $y_n=(2n-1)/(2n)$ and $c=1-1/n$. The corresponding

$$\mathcal{Y}^* = \left\{\left(\frac{1}{2n},\frac{2n-1}{2n}\right),\left(\frac{3}{2n},\frac{2n-3}{2n}\right),\dots,\left(\frac{2n-1}{2n},\frac{1}{2n}\right)\right\}$$

and ML1D($\mathcal{Y}^*$) $=1/2n$. Therefore, the desired conclusion holds for size n. ■

Proof of Theorem 4.5: For $p=3$ and $m\ge 1$, the simplex-lattice design $\mathcal{D}$ has $n=\binom{p+m-1}{m}=(m+2)(m+1)/2$ points, denoted as $\{\boldsymbol{y}_1,\dots,\boldsymbol{y}_n\}$, and these points are all possible combinations of the components under the constraint $x_1+x_2+x_3=1$, and each component is an element from the set $\{0,1/m,2/m,\dots,1\}$. For a given contraction ratio $\rho\in(0,1]$ and a vector component $x=i/m, 0\le i\le m$, the contracted component is

$$x' = \rho x + (1-\rho)/3 = 1/3 + (i/m - 1/3)\rho.$$

By this formula we can easily obtain the coordinates of the Scheffé-type simplex-lattice design $\mathcal{D}_\rho=\{\boldsymbol{y}_1,\dots,\boldsymbol{y}_n\}$.

The region of T^3 can be decomposed into n distinct parts (Voronoi cells) such that each of these parts contains all points that are closer to $\boldsymbol{y}_i$ under the L_1-distance, $i=1,\dots,n$. In other words, each of the Voronoi cell contains a single point $\boldsymbol{y}_i$, $i=1,\dots,n$, and we denote it as T_i^3. For any point $\boldsymbol{x}\in T_i^3$, $\min_{1\le j\le n} D_{l_1}(\boldsymbol{x},\boldsymbol{y}_j)=D_{l_1}(\boldsymbol{x},\boldsymbol{y}_i)$.

As an illustration, Figure A1 shows the 10 points of a Scheffé type $\{3,3\}$-simplex-lattice design and the corresponding Voronoi cells.

Under the L_1-metric on T^3, we can deduce that the regions (Voronoi cells) $V_i, i=1,\dots,n$ are polygons and can be classified into three categories by symmetry of $\mathcal{D}$, as illustrated in Figure A1 for the case of $m=3$. Consequently, to compute ML1D($\mathcal{D}_\rho$), we only need to consider three points of $\mathcal{D}_\rho$:

$$\boldsymbol{y}_1 = \left(\frac{1}{3}+\frac{2\rho}{3}, \frac{1}{3}-\frac{\rho}{3}, \frac{1}{3}-\frac{\rho}{3}\right),$$
$$\boldsymbol{y}_2 = \left(\frac{1}{3}+\left(\frac{2}{3}-\frac{1}{m}\right)\rho, \frac{1}{3}-\frac{\rho}{3}, \frac{1}{3}+\left(\frac{1}{m}-\frac{1}{3}\right)\rho\right),$$
$$\boldsymbol{y}_3 = \left(\frac{1}{3}+\left(\frac{2}{3}-\frac{2}{m}\right)\rho, \frac{1}{3}+\left(\frac{1}{m}-\frac{1}{3}\right)\rho, \frac{1}{3}+\left(\frac{1}{m}-\frac{1}{3}\right)\rho\right),$$

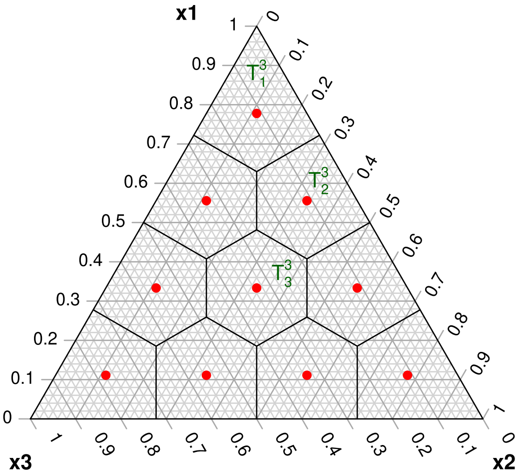

Figure A1. A contracted Scheffé type {3, 3}-simplex-lattice design.

and their corresponding regions T_i^3, as labelled in Figure A1 for the case of $m = 3$. We have $\mathrm{ML1D}(\mathcal{D}_\rho) = E_{\boldsymbol{X}}[\min_{1\le j\le (m+2)(m+1)/2} D_{l_1}(\boldsymbol{X}, \boldsymbol{y}_j)]$ which is equal to

$$3\int_{\boldsymbol{x}\in T_1^3} D_{l_1}(\boldsymbol{x},\boldsymbol{y}_1)\,\mathrm{d}\mu(\boldsymbol{x}) + (3m-3)\int_{\boldsymbol{x}\in T_2^3} D_{l_1}(\boldsymbol{x},\boldsymbol{y}_2)\,\mathrm{d}\mu(\boldsymbol{x}) + \frac{(m-1)(m-2)}{2}\int_{\boldsymbol{x}\in T_3^3} D_{l_1}(\boldsymbol{x},\boldsymbol{y}_3)\,\mathrm{d}\mu(\boldsymbol{x}),$$

where $\boldsymbol{X} \sim U(T^3)$ and μ is the uniform probability measure on T^3.

By a careful check, we can obtain that the region

$$T_1^3 = \left\{(x_1,x_2,x_3) : x_1 = 1 - x_2 - x_3, 0 \le x_2, x_3 \le 1, x_1 - x_2 \ge \frac{m-1}{m}\rho, x_1 - x_3 \ge \frac{m-1}{m}\rho\right\},$$

and is equivalent to

$$V_1^2 := \left\{(x_2,x_3) : 0 \le x_2 \le \frac{1}{2} - \frac{m-1}{2m}\rho, 0 \le x_3 \le \frac{1}{2} - \frac{m-1}{2m}\rho, 2x_2 + x_3 \le 1 - \frac{m-1}{m}\rho, x_2 + 2x_3 \le 1 - \frac{m-1}{m}\rho\right\}.$$

The region

$$T_2^3 = \{(x_1,x_2,x_3) : x_1 = 1 - x_2 - x_3, 0 \le x_2, x_3 \le 1, \frac{m-3}{m}\rho \le x_1 - x_3 \le \frac{m-1}{m}\rho, x_1 - x_2 \ge \frac{m-2}{m}\rho, x_3 - x_2 \ge 0\right\},$$

and is equivalent to

$$V_2^2 = \left\{(x_2,x_3) : x_3 \ge x_2 \ge 0, 1 - \frac{m-1}{m}\rho \le x_2 + 2x_3 \le 1 - \frac{m-3}{m}\rho, 2x_2 + x_3 \le 1 - \frac{m-2}{m}\rho\right\}.$$

The region

$$T_3^3 = \{(x_1,x_2,x_3) : x_1 = 1 - x_2 - x_3, 0 \le x_2, x_3 \le 1, \frac{m-4}{m}\rho \le x_1 - x_2 \le \frac{m-2}{m}\rho, \frac{m-4}{m}\rho \le x_1 - x_3 \le \frac{m-2}{m}\rho, -\frac{\rho}{m} \le x_2 - x_3 \le \frac{\rho}{m}\right\},$$

and is equivalent to

$$V_3^2 = \left\{(x_2, x_3) : 1 - \frac{m-2}{m}\rho \le 2x_2 + x_3 \le 1 - \frac{m-4}{m}\rho, 1 - \frac{m-2}{m}\rho \le x_2 + 2x_3 \le 1 - \frac{m-4}{m}\rho, -\frac{\rho}{m} \le x_2 - x_3 \le \frac{\rho}{m}\right\}.$$

Since $(X_1, X_2, X_3) \sim U(T^3)$, $(X_2, X_3) \sim U(V^2)$ and (X_2, X_3) has a probability density function $2!1_{(x_2,x_3)\in V^2}$ by Lemma 2.2 where $V^2 = \{(x_2, x_3) : x_2, x_3 \ge 0, x_2 + x_3 \le 1\}$, we have $\mathrm{ML1D}(\mathcal{D}_\rho)$ is equal to

$$\begin{aligned}
&6\int_{(x_2,x_3)\in V_1^2} \left(\left|x_2 - \frac{1-\rho}{3}\right| + \left|x_3 - \frac{1-\rho}{3}\right| + \left|x_2 + x_3 - \frac{2-2\rho}{3}\right|\right) \mathrm{d}x_2 \mathrm{d}x_3 \\
&+ (6m-6)\int_{(x_2,x_3)\in V_2^2} \left(\left|x_2 - \frac{1-\rho}{3}\right| + \left|x_3 - \frac{1}{3} - \left(\frac{1}{m} - \frac{1}{3}\right)\rho\right|\right. \\
&\left.+ \left|x_2 + x_3 - \frac{2}{3} + \left(\frac{2}{3} - \frac{1}{m}\right)\rho\right|\right) \mathrm{d}x_2 \mathrm{d}x_3 \\
&+ (m-1)(m-2)\int_{(x_2,x_3)\in V_3^2} \left(\left|x_2 - \frac{1}{3} - \left(\frac{1}{m} - \frac{1}{3}\right)\rho\right| + \left|x_3 - \frac{1}{3} - \left(\frac{1}{m} - \frac{1}{3}\right)\rho\right|\right. \\
&\left.+ \left|x_2 + x_3 - \frac{2}{3} + \left(\frac{2}{3} - \frac{2}{m}\right)\rho\right|\right) \mathrm{d}x_2\, \mathrm{d}x_3.
\end{aligned}$$

Tedious calculations show

$$\mathrm{ML1D}(\mathcal{D}_\rho) = \begin{cases} \dfrac{\rho^3}{m^2} + \dfrac{7\rho^3}{9m} + \dfrac{2}{27}(\rho-1)^2(\rho+8), & \text{if } 0 \le \rho \le \dfrac{m}{m+3}, \\ -\dfrac{m^2(\rho-1)^3 + m(7\rho-16)(\rho-1)^2 + 3\rho^2(2\rho-9)}{27m}, & \text{if } \dfrac{m}{m+3} \le \rho \le 1. \end{cases}$$

It can be checked that when $\rho = 0$, $\mathcal{D}_\rho$ reduces to $\{(1/3, 1/3, 1/3)\}$, i.e., the centre point of T^3, and $\mathrm{ML1D}(\mathcal{D}_\rho) = 16/27$, which is the same as Example 4.2. Taking the derivative of $\mathrm{ML1D}(\mathcal{D}_\rho)$ with respect to ρ, we have the local minimum is attained at

$$\rho^* = \frac{m^2 - \sqrt{21m^2 + 102m + 81} + 10m + 9}{m^2 + 7m + 6}$$

and the corresponding

$$\mathrm{ML1D}(\mathcal{D}_{\rho^*}) = \frac{7m^3 + 145m^2 - (14m+54)\sqrt{21m^2 + 102m + 81} + 624m + 486}{9m(m+1)(m+6)^2}.$$

It can be verified that this is a global minimum value of $\mathrm{ML1D}(\mathcal{D}_\rho)$ over $\rho \in (0, 1]$, which completes the proof. ■

Appendix 2. Additional tables and figures

In Tables A1–A4, we list the simplex-lattice designs, the optimal Scheffé-type simplex-lattice designs and ML1D-RPs (generated by Algorithm 3) for $p = 3, n = 3, 6, 10, 15$, respectively. Figure A2 provides a visualization of ML1D-RPs on T^3 for $p = 3, n = 4, \ldots, 15$.

Table A1. List of the simplex-lattice designs, the optimal Scheffé-type simplex-lattice designs and ML1D-RPs, where $p = 3, n = 3, N = 100{,}000$.

	Simplex-lattice			Optimal Scheffé-type simplex-lattice			ML1D-RPs		
	x1	x2	x3	x1	x2	x3	x1	x2	x3
1	1	0	0	0.6055782	0.1972109	0.1972109	0.6098006	0.1943938	0.1958057
2	0	1	0	0.1972109	0.6055782	0.1972109	0.1950331	0.6109516	0.1940154
3	0	0	1	0.1972109	0.1972109	0.6055782	0.1934008	0.1943805	0.6122187

Table A2. List of the simplex-lattice designs, the optimal Scheffé-type simplex-lattice designs and ML1D-RPs, where $p = 3, n = 6, N = 100{,}000$.

	Simplex-lattice			Optimal Scheffé-type simplex-lattice			ML1D-RPs		
	x1	x2	x3	x1	x2	x3	x1	x2	x3
1	1.0	0.0	0.0	0.7164063	0.1417968	0.1417968	0.4289461	0.1449483	0.4261055
2	0.5	0.5	0.0	0.4291016	0.4291016	0.1417968	0.7250440	0.1381427	0.1368133
3	0.0	1.0	0.0	0.1417968	0.7164063	0.1417968	0.1450585	0.4277576	0.4271839
4	0.5	0.0	0.5	0.4291016	0.1417968	0.4291016	0.1371071	0.1374333	0.7254596
5	0.0	0.5	0.5	0.1417968	0.4291016	0.4291016	0.1366079	0.7245433	0.1388488
6	0.0	0.0	1.0	0.1417968	0.1417968	0.7164063	0.4266384	0.4308233	0.1425384

Table A3. List of the simplex-lattice designs, the optimal Scheffé-type simplex-lattice designs and ML1D-RPs, where $p = 3, n = 10, N = 100{,}000$.

	Simplex-lattice			Optimal Scheffé-type simplex-lattice			ML1D-RPs		
	x1	x2	x3	x1	x2	x3	x1	x2	x3
1	1.0000000	0.0000000	0.0000000	0.7777778	0.1111111	0.1111111	0.1120330	0.5597077	0.3282594
2	0.6666667	0.3333333	0.0000000	0.5555556	0.3333333	0.1111111	0.3314367	0.3356061	0.3329572
3	0.3333333	0.6666667	0.0000000	0.3333333	0.5555556	0.1111111	0.5595401	0.3278520	0.1126079
4	0.0000000	1.0000000	0.0000000	0.1111111	0.7777778	0.1111111	0.1059066	0.1075473	0.7865461
5	0.6666667	0.0000000	0.3333333	0.5555556	0.1111111	0.3333333	0.5529791	0.1123789	0.3346420
6	0.3333333	0.3333333	0.3333333	0.3333333	0.3333333	0.3333333	0.3348998	0.5544492	0.1106510
7	0.0000000	0.6666667	0.3333333	0.1111111	0.5555556	0.3333333	0.3292527	0.1133453	0.5574020
8	0.3333333	0.0000000	0.6666667	0.3333333	0.1111111	0.5555556	0.1075149	0.7859533	0.1065318
9	0.0000000	0.3333333	0.6666667	0.1111111	0.3333333	0.5555556	0.7869565	0.1050513	0.1079922
10	0.0000000	0.0000000	1.0000000	0.1111111	0.1111111	0.7777778	0.1118170	0.3317011	0.5564819

Table A4. List of the simplex-lattice designs, the optimal Scheffé-type simplex-lattice designs and ML1D-RPs, where $p = 3, n = 15, N = 100{,}000$.

	Simplex-lattice			Optimal Scheffé-type simplex-lattice			ML1D-RPs		
1	1.00	0.00	0.00	0.8170291	0.0914854	0.0914854	0.0849448	0.8267691	0.0882861
2	0.75	0.25	0.00	0.6356432	0.2728714	0.0914854	0.8250552	0.0873248	0.0876199
3	0.50	0.50	0.00	0.4542573	0.4542573	0.0914854	0.2720759	0.4556800	0.2722442
4	0.25	0.75	0.00	0.2728714	0.6356432	0.0914854	0.0910114	0.4494894	0.4594992
5	0.00	1.00	0.00	0.0914854	0.8170291	0.0914854	0.2753537	0.2703635	0.4542828
6	0.75	0.00	0.25	0.6356432	0.0914854	0.2728714	0.2718051	0.0909173	0.6372776
7	0.50	0.25	0.25	0.4542573	0.2728714	0.2728714	0.4530971	0.2734095	0.2734934
8	0.25	0.50	0.25	0.2728714	0.4542573	0.2728714	0.0917261	0.6346769	0.2735970
9	0.00	0.75	0.25	0.0914854	0.6356432	0.2728714	0.4566436	0.0898462	0.4535101
10	0.50	0.00	0.50	0.4542573	0.0914854	0.4542573	0.0946925	0.2644619	0.6408456
11	0.25	0.25	0.50	0.2728714	0.2728714	0.4542573	0.6375184	0.0927961	0.2696855
12	0.00	0.50	0.50	0.0914854	0.4542573	0.4542573	0.6354206	0.2712685	0.0933109
13	0.25	0.00	0.75	0.2728714	0.0914854	0.6356432	0.0877902	0.0857171	0.8264927
14	0.00	0.25	0.75	0.0914854	0.2728714	0.6356432	0.2667695	0.6419888	0.0912417
15	0.00	0.00	1.00	0.0914854	0.0914854	0.8170291	0.4515644	0.4578724	0.0905632

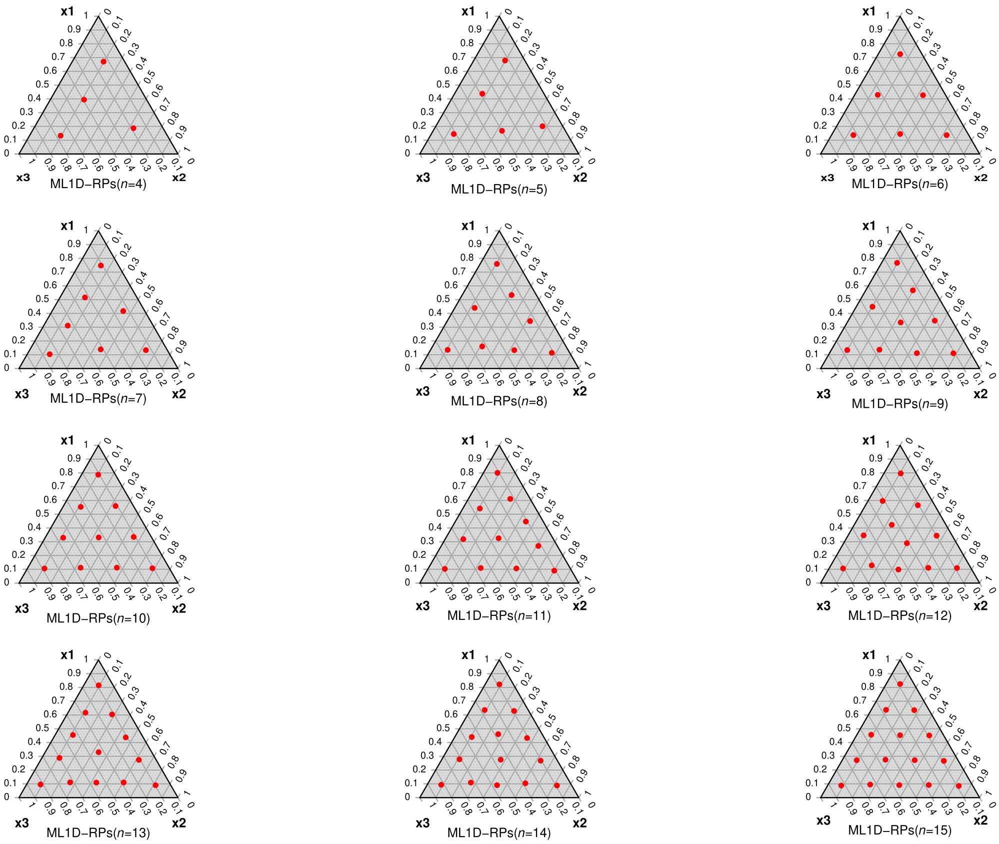

Figure A2. Visualization of the patterns of ML1D-RPs ($p = 3, n = 4, \ldots, 15, N = 100{,}000$).

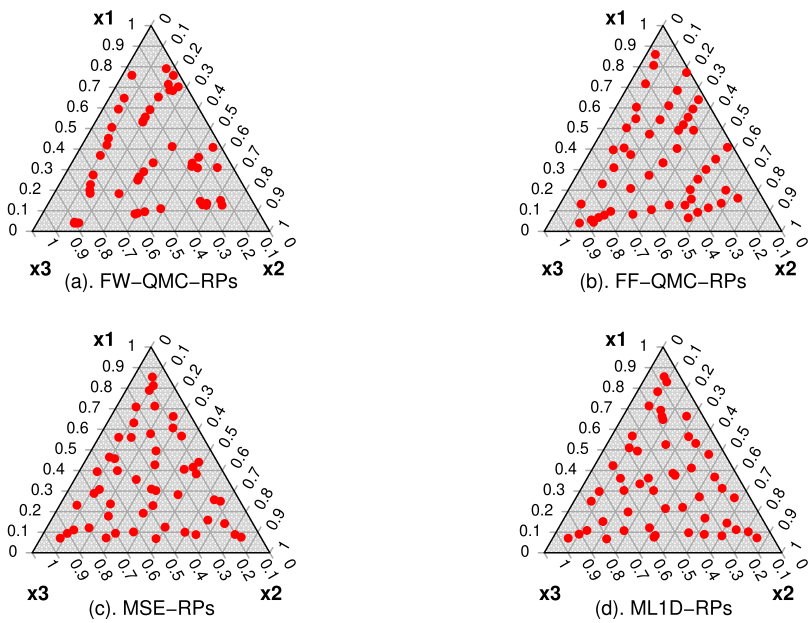

Figure A3. Four types of representative points projected onto the first three dimensions($n = 50, p = 4$).

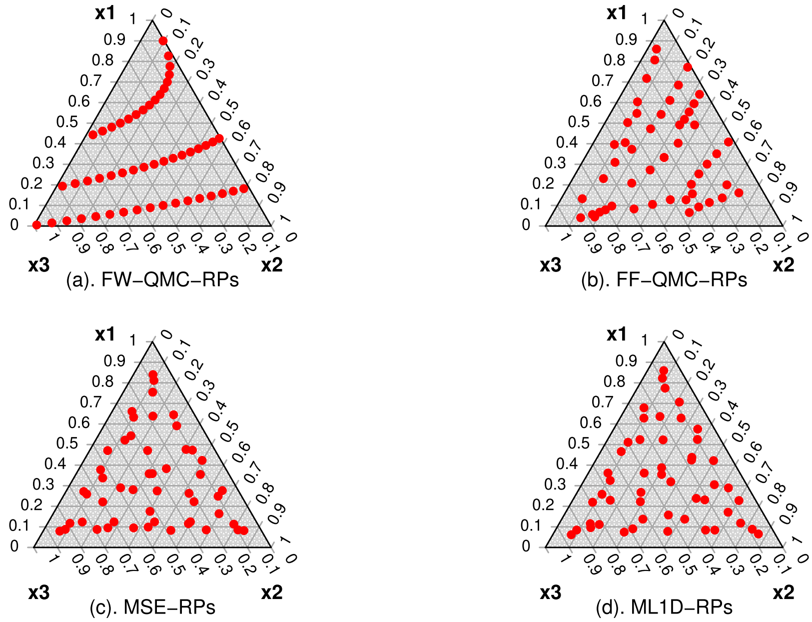

Figure A4. Four types of representative points projected onto the last three dimensions($n = 50, p = 4$).

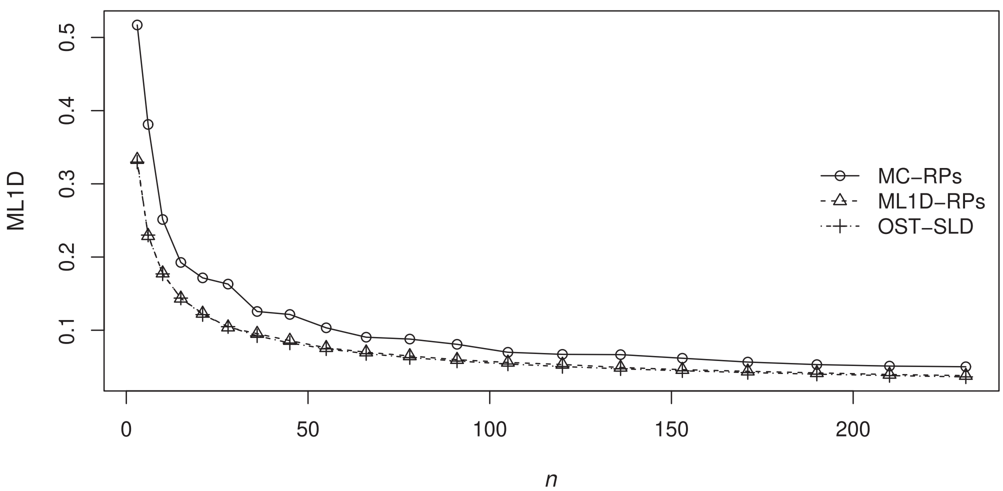

Figure A5. Mean L_1-distance (ML1D) criterion values for MC-RPs, ML1D-RPs, OST-SLD as n increases ($n = \binom{p+m-1}{m}, m = 1, \ldots, 20, p = 3$).